Spectral Bidirectional Reflectance Factor Measurements of Two Dwarf Shrub Species

Petri Forsström

School of Electrical Engineering

Thesis submitted for examination for the degree of Master of Science in Technology.

Espoo 19 January 2018

Supervisor:

Prof. Miina Rautiainen, Aalto University

Advisor:

PhD Jouni Peltoniemi, Finnish Geospatial Research Institute

Aalto University
School of Electrical Engineering

AALTO UNIVERSITY
SCHOOL OF ELECTRICAL ENGINEERING

ABSTRACT OF THE
MASTER'S THESIS

Author: Petri Forsström

Title: Spectral bidirectional reflectance factor measurements of two dwarf shrub species

Date: 19.1.2018 Language: English Number of pages: 7+62

Department of Electronics and Nanoengineering

Professorship: Space Science and Technology

Supervisor: Prof. Miina Rautiainen

Advisor: PhD Jouni Peltoniemi

Recent studies have shown the benefits of multiangular remote sensing techniques for characterizing vegetation reflection properties. The study of spectral anisotropy of understory vegetation enables methods for improved plant species identification, and provides valuable input data for radiation scattering models of forests. This thesis presents the applied methods and results of a research effort carried out over the growing season of 2017 for the temporal spectral characterization of two of the economically most important wild berry species in Finland: lingonberry (*Vaccinium vitis-idaea*) and blueberry (*Vaccinium myrtillus*).

The spectral bidirectional reflectance factor (BRF) data on lingonberry and blueberry shrub samples were collected in a multidirectional measurement geometry using the Finnish Geodetic Institute Goniospectrometer (FIGIFIGO) in laboratory conditions. Leaf reflectance and transmittance spectra on both species were collected with SpectroClip-TR spectral probe. The anisotropic characteristics were analysed in the spectral range from 400 to 2200 nm for view angle dependence (-40° to +40°), illumination angle dependence (+40°, +55°), seasonal dynamics over the growing season (2017), and for berry and flower detection.

Both lingonberry and blueberry shrubs have strong backward and notable forward scattering characteristics on the principal plane. In the interspecies comparison, lingonberry is brighter into all view direction in the visible and near infrared wavelengths but darker in the short-wave infrared. Increasing the illumination zenith angle by 15° improves the spectral discrimination of the two dwarf shrub species by inducing a 12% ratio of the spectral responses. Vegetation indices that are commonly used in remote sensing of forests (NDVI, NDVI705, MSI, PSRI) show low sensitivity to the changes in the view- and illumination angles. The presence of lingonberries and lingonberry flowers is indicated as a spectral peak around 679 nm in the spectral ratio of samples with berries or flowers to samples without berries or flowers.

It was shown that the analysis of spectral data on the reflectance anisotropy improves the spectral discrimination of the dwarf shrub species. The contribution of the berries on the obtained shrub spectra was shown to be notable enough to justify further studies by applying unmanned aerial vehicle (UAV) platforms. Future studies on the aerial spectral data are suggested to evaluate the potential of berry mapping in larger-scale.

Keywords: BRF, reflectance factor, remote sensing, FIGIFIGO, anisotropy

AALTO-YLIOPISTO
SÄHKÖTEKNIIKAN KORKEAKOULU

DIPLOMITYÖN
TIIVISTELMÄ

Tekijä: Petri Forsström

Työn nimi: Kahden varpukasvin spektrien kaksisuuntaiset heijastussuhdetekijämittaukset

Päivämäärä: 19.1.2018 Kieli: Englanti Sivumäärä: 7+62

Elektroniikan ja nanotekniikan laitos

Professuuri: Avaruustekniikka ja -tiede

Työn valvoja: Prof. Miina Rautiainen

Työn ohjaaja: FT Jouni Peltoniemi

Viimeaikaiset tutkimukset ovat osoittaneet monisuunta-spektrometrian hyödyt kasvillisuuden heijastusominaisuuksien karakterisoinnissa kaukokartoituksessa. Aluskasvillisuuden spektrien anisotropian tutkiminen edesauttaa kehittämään menetelmiä kasvilajien tunnistamiseksi ja tarjoaa validointiaineistoa metsien sirontamalleihin. Tämä diplomityö esittää menetelmät ja tulokset Suomen kahden taloudellisesti tärkeimmän luonnonmarjoja tuottavan varpukasvin, mustikan (*Vaccinium myrtillus*) ja puolukan (*Vaccinium vitis-idaea*), spektrien temporaalisesta karakterisointikampanjasta kasvukauden 2017 yli.

Kaksisuuntainen heijastussuhdetekijä spektriaineisto mitattiin mustikan ja puolukan varpunäytteistä monisuuntamittausgeometriassa FIGIFIGO (Finnish Geodetic Institute Goniospectrometer) goniospektrometrillä laboratorio-olosuhteissa. Lehtien heijastus- ja läpäisyspektrit mitattiin molemmista lajeista käyttäen SpectroClip-TR mittalaitetta. Anisotropiset ominaispiirteet analysointiin aallonpituuksien 400 - 2200 nm välillä katselukulmariippuvuudelle (-40° to +40°), valaistuskulmariippuvuudelle (+40°, +55°), vuodenajan aiheuttamille muutoksille (kasvukausi 2017) sekä marja ja kukintojen tunnistamiselle.

Sekä puolukka että mustikka osoittavat voimakasta taaksepäin suuntautuvaa ja huomattavaa eteenpäin suuntautuvaa ominaissirontaa päätasossa. Lajien välisessä vertailussa puolukka on kirkkaampi kaikkiin mitattuihin katselukulmiin näkyvän valon ja lähi-infrapunan aallonpituuksilla, mutta tummempi lyhytaaltoisen infrapunan alueella. Valaistuskulman zeniitin kasvattaminen 15° parantaa lajien spektrien erotettavuutta aiheuttamalla 12 %:n eron lajien heijastusvasteisiin. Yleisesti metsän kaukokartoituksessa käytetyt kasvillisuusindeksit (NDVI, NDVI705, MSI, PSRI) osoittavat matalaa herkkyyttä katselu- ja valaistuskulman muutoksille. Näytteessä olevat puolukanmarjat ja -kukat erottuvat spektrissä piikkinä 679 nm:n kohdalla, kun tarkastellaan marjallisten ja kukallisten näytteiden suhdetta marjattomiin ja kukattomiin.

Spektriaineiston heijastus-anisotropian analysoinnin näytettiin edesauttavan varpukasvien erotettavuutta. Marjojen vahva kontribuutio varpunäytteistä mitattuihin spektreihin osoitettiin niin selkeästi, että jatkotutkimuksia UAV (unmanned aerial vehicle) -alustalla voidaan pitää perusteltuina. Ilma-aluksilla kerättyä aineistoa ehdotetaan käytettävän marjojen laajemman kartoituksen potentiaalin selvittämiseksi.

Avainsanat: BRF, heijastussuhdetekijä, kaukokartoitus, FIGIFIGO, anisotropia

Preface

I would like to thank my supervising Professor Miina Rautiainen for her support and for introducing me to the fascinating world of Earth observation. I would also like to thank my advisor Jouni Peltoniemi at Finnish Geodetic Research Institute for giving me the possibility to undertake this project and for his inspiring guidance.

I acknowledge as well the help and expertise of researchers Juha Suomalainen, Teemu Hakala, and Aarne Hovi.

This research has been supported and facilitated by Finnish Geodetic Research Intitute and Aalto University.

Finally, I would like to thank my family for their continuous support in my studies.

Otaniemi, 19.1.2018

Petri Forsström

Contents

List of abbreviations

ANIF	Anisotropy factor
ANIX	Anisotropy index
ASD	Analytical Spectral Devices, Inc
ASG	Automated Spectro-Goniometer
B	Blueberry shrub sample
BRDF	Bidirectional reflectance distribution function
BRF	Bidirectional reflectance factor
CHRIS	Compact High Resolution Imaging Spectrometer
DOY	Day of Year
EGO	European Optical Goniometric Facility
FGI	Finnish Geospatial Research Institute
FIGIFIGO	Finnish Geodetic Institute Field Goniospectrometer
FIGOS	Field-Goniometer System
GRIT-T	Goniometer of the Rochester Institute of Technology-two
L	Lingonberry shrub sample
LAI	Leaf area index
MISR	Multi-angle Imaging SpectroRadiometer
MODIS	Moderate Resolution Imaging Spectroradiometer
MSI	Moisture stress index
NDVI	Normalized difference vegetation index
NDVI705	Red-edge normalized difference vegetation index
NIR	Near-infrared
PARABOLA III	Portable Apparatus for Rapid Acquisition of Bidirectional Observation of the Land and Atmosphere III
POLDER	POLarization and Directionality of the Earth's Reflectances
pp	Principal plane
PROBA-1	Project for On-Board Autonomy
PSRI	Plant senescence reflectance index
SFG	Sandmeier Field Goniometer
SWIR	Short-wave infrared
UAV	Unmanned aerial vehicle
ULGS	University of Lethbridge Goniometer System
VIS	Visible spectrum
VNIR	Visible and near-infrared

Symbols

Quantity	Symbol	Unit
Absorbed radiation (fraction)	a	[ ]
Diameter	d	[m]
Footprint length	l	[m]
Illumination azimuth angle	ϕ_r	[°]
Illumination zenith angle	θ_r	[°]
Radiant flux	Φ	[W]
Reflectance factor	R	[ ]
Reflected radiation (fraction)	r	[ ]
Sensor azimuth angle	ϕ_r	[°]
Sensor zenith angle	θ_r	[°]
Spectral irradiance	E_λ	[W m^{-2} nm^{-1}]
Spectral radiance	L_λ	[W m^{-2} sr^{-1} nm^{-1}]
Transmitted radiation (fraction)	τ	[ ]

1 Introduction

1.1 Motivation

The Earth is a living planet, with large part of its total land area covered in dynamic green vegetation. This vegetation produces constantly oxygen and moisture into the atmosphere while reducing the amounts of harmful atmospheric substances, such as carbon dioxide. Due to human activity the average temperature in Finland has increased more than 2.3°C from the times of industrial revolution [1] and is predicted to continue its climb at least until 2060 [2]. The resulting reduction of snow cover during the winters and the lengthening of the summers affect strongly on the animal and plant life alike which either adapts, moves, or perishes, while new species move further north with an increasing strain on the existing nature. While most of the effects of climate change have undeniably negative impacts on life in the northern hemisphere, new business and recreational possibilities may arise from temporally longer growing seasons that induce higher yields from crops, trees, and other producing plants.

1.2 Research objective

This thesis gives a detailed description of a spectral research effort carried out over the growing period of 2017. The collected remote sensing ground truth data represents the reflectance characteristics of two dwarf shrub species, free of environmental and atmospheric spectral effects. The spectral anisotropy characteristics of natural state wild lingonberry (*Vaccinium vitis-idaea*) and blueberry (*Vaccinium myrtillus*) were analysed from spectral bidirectional reflectance factor (BRF) measurements. The measurements were made in a multidirectional measurement geometry under two distinct illumination directions. The applied illumination angles represent solar elevations during the summer months in the southern Finland latitudes, and thus extends the usage of the data in multitemporal applications. Ancillary data, in form of single leaf scattering spectra were collected to enable a component wise analysis of the shrub samples, and a spectral analysis of the seasonal changes in the leaves. Furthermore, the collected spectral data is made available for others to utilize in future studies. The instruments used to carry out the measurements were Finnish Geodetic Institute Field Goniospectrometer (FIGIFIGO) provided by Finnish Geospatial Research Institute (FGI), and SpectroClip-TR manufactured by OceanOptics and provided by Aalto University.

The goal of this study was to find answers to the following three research questions and to evaluate the significance and usefulness of the results for future studies:

- Are there characteristic spectral anisotropy differences between blueberry and lingonberry shrubs?

- What are the seasonal changes in BRF of blueberry and lingonberry considering the different phenological stages?

- Can the dwarf shrub flowers and berries be detected from measured spectra using FIGIFIGO measurements? Does collecting single leaf reflectance spectra with SpectroClip-TR improve this?

As of today, I am not aware of a presiding study on any forest understory species that has addressed a set of research questions as comprehensive as the one presented here. Therefore, the data presented in this thesis are considered valuable for future studies in e.g. improving and validating radiation scattering models of forests, as ground truth reference data for future remote sensing berry detection applications, and as input data for statistical models for predicting annual berry yield.

1.3 Species overview and exploitation in Finland

Lingonberry and blueberry are both *Vaccinium* genus dwarf shrubs belonging to *Ericaceae* (heath) family (Figure 1). Both species have a wide geographical distribution in Finland with annual estimated berry yields of 244 million kg for lingonberry and 168 million kg for blueberry [3]. Somewhat broader estimates for annual berry yields range from 180 to 200 million kg for lingonberry (with 500 million kg a possibility) and 150 to 250 million kg for blueberry [4]. The picking percentages vary between 3% and 10%, leaving the bulk of the yield in the forest uncapitalized. Of the picked berries, approximately three fourths go directly to private use and the rest are sold as processed product such as jams, juices and beverages [5]. A small percentage is also exported from Finland, with the most common product being frozen blueberries [5].

Both species grow in dry boreal forests usually dominated by pines, allowing lots of light to reach the forest floor. Lingonberry is a broad-leaved evergreen species, usually 5 to 30 cm (up to 50 cm) tall keeping its thick waxy leaves in normal conditions over the winter months. Blueberry grows typically 15 to 50 cm (up to 70 cm) tall and is a deciduous species dropping its leaves in the autumn. Lingonberry has 8 to 30 mm long oval shaped leaves with downward curling edges, green adaxial (upper) side, and light green abaxial (lower) side. Lingonberry leaves are thick and stiff, distributed radially around the plant stem. Blueberry leaves are 8 to 25 mm long, saw edged and more almond shaped. Compared to lingonberry leaves, blueberry leaves are thinner, translucent and more flexible. The distribution of blueberry leaves is more sparse within a complex branched blueberry stem structure. [6]

Lingonberry bears clustered flowers from mid-summer to late July. The clusters contain typically 5 to 10 white-pink coloured 5 mm long flowers. Blueberry bears berry-shaped, individually distributed reddish flowers from early summer to mid-summer. Lingonberries are produced from flowers in late August or early September and blueberries in late July or early August. Both species' berries contain a fleshy juicy pulp indicating a large relative water content. The sizes of the berries on both species vary typically between 5 to 8 mm. Lingonberries are bright red in colour while blueberries are indigo-coloured. Blueberries have a noticeable loose waxy layer (a bloom) on top of the berry skin that protects the berry from insects and reduces the loss of moisture.

Lingonberries and blueberries are both highly regarded for their health benefits which have been thoroughly studied. Berries contain vitamins, fibres, minerals, and flavonoid compounds such as antioxidants with known antibacterial activity and thus positive health effects. [7]

Figure 1. A collection of photographs showing (a) lingonberry shrubs, (b) picked lingonberries, (c) blueberry shrubs, and (d) picked blueberries.

2 Background

2.1 Optical properties of vegetation

Through evolution, human eyes have developed a sensitivity to an electromagnetic radiation of varying intensity, contained within a 400 nm wide band in the electromagnetic radiation spectrum, referred to as visible spectrum. A passive remote sensing instruments capable of recoding the incident energy in the same wavelengths as our eyes but with an extended range into short-wave infrared region can be considered as an extension of our natural vision. In many cases it is much more intuitive to make interpretations from an image acquired using an optical imaging instrument than from one acquired using e.g. imaging radar. The advantages for observing the Earth in optical range arise from the characteristic distribution of solar energy in the Sun's irradiance spectrum, the spectral response of the vegetation to the incident solar radiation, and the fact that in the optical spectral range sensitive and accurate sensors are relatively cheap to manufacture.

Due to the spectral characteristics of the solar radiation spectrum and the spectral absorption and scattering characteristics of the Earth's atmosphere, the irradiance peak at sea level sets roughly between wavelengths 400 and 700 nm. Through evolutional iterations, green leaved vegetation has developed means for exploiting this energy through a process called photosynthesis. Photosynthesis is a conversion of electromagnetic energy into chemical energy from which the end-product is glucose, a simple sugar used by the plant to power growth. Photosynthesis is enabled by electron excitation of chlorophyll molecules (ions of the pigments) by the energy in the incident radiation. The chlorophyll pigments absorb efficiently red and blue colour light which through light dependent and independent chemical processes produces glucose for the plant while splitting water molecules into hydrogen and oxygen. [8]

Three well-known optical interaction properties between the incident electromagnetic radiation field and the matter lay the basis for optical remote sensing data analysis: reflection, transmission and absorption [8]. These optical properties can be determined by applying spectral remote sensing measurements techniques for observing the amount of radiation scattered or transmitted into the direction of the sensor. Instruments have physical constrains that limit the measurements of these quantities and typically only reflectance data is collected, and only from nadir view. Assumption of these properties are needed as input for radiative transfer models. With suitable instrumentation, it is possible to obtain well approximated information on the reflectance anisotropy describing the optical properties of the scattering body. These data can be used to improve the models.

Passive remote sensing systems typically measure solar radiation after several interactions within the medium and the target of interest. This study limits its scope to electromagnetic spectrum between the visible and short-wave infrared wavelengths where the measured energy is scattered light originating from an artificial source imitating the Sun's irradiance spectrum.

As the incident energy contained in the electromagnetic radiation field reaches a plant leaf, the leaf, as a system, can either partly or completely intercept the radiation. The fraction of the incident radiation that does not interact with the leaf is transmitted through. Law of conservation of energy states that the total energy is preserved. Thus, the total interaction can be described as a sum of the fractions of the total interaction as in Equation 1 [8]:

$$\Phi_{i,\lambda} = \Phi_{a,\lambda} + \Phi_{r,\lambda} + \Phi_{\tau,\lambda} = a_\lambda \Phi_i + r_\lambda \Phi_i + \tau_\lambda \Phi_i \,, \quad (1)$$

or in Equation 2:

$$a_\lambda + r_\lambda + \tau_\lambda = 1 \,, \quad (2)$$

where Φ is the incident radiant flux [W] reaching the leaf, a is the absorbed fraction, r the reflected fraction, and τ is the transmitted fraction. Each fraction has a characteristic directional and spectral dependence. This spectral dependence is the core property exploited in all remote sensing. A graphical representation of the spectral fractioning of the incident radiation is shown in Figure 2.

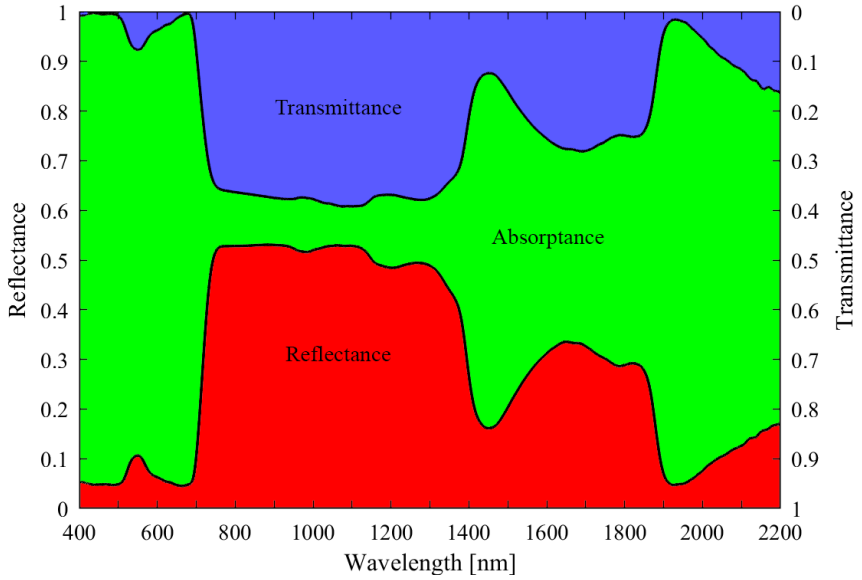

Figure 2. Three possible spectral interactions of green leaf to incident shortwave radiation: reflectance (red), transmittance (blue), and absorptance (green) as a function of wavelength. The data are examples of those measured from lingonberry leaves.

2.2 Reflectance theory

Measurement environment, with all its contributing elements along with the directional properties of the illumination and the sensor, define the existing measurement geometry, and thus the measured reflectance quantity. The sensor measures spectral radiance, L [W m^{-2} sr^{-1} nm^{-1}] which is the spectral radiant flux [W nm^{-1}] contained in the projected source area in the beam geometry [m^2] into a solid angle towards a specific direction [sr]. If no interactions occur between the scatterer and sensor, radiance is always constant regardless

of the separating distance. When radiance is integrated over the hemisphere the resulting quantity is called spectral irradiance, E [W m^{-2} nm^{-1}] which can be used to characterize the illumination source. Radiance and irradiance can be measured using instruments such as spectroradiometers. The obtained measure of radiance can be further developed into physical quantities such as reflectance and reflectance factor.

Reflectance and reflectance factor should be evaluated in associated geometrical domain, defined by the illumination and sensor geometries of the measurement setup. Three basic geometries used in literature to describe the geometrical domain are directional, conical, and hemispherical (Figure 3). The related reflectance quantities are some combination of these geometries. Bidirectional geometry is always a conceptual quantity since it is defined for infinitesimal solid angles. Therefore, the true measurable reflectance quantities are always in either conical or hemispherical domains. Conical-conical is typical laboratory measurements where the illumination is considered as non-ideal beam and e.g. a goniospectrometer is used to determine the angular distribution of the scattered light. Outdoor measurements made under natural solar illumination have always a hemispherical illumination geometry due to light scattering in the ambient atmosphere. Because of the mentioned limitations related to real measurements, the measurement setup geometries are reduced to four possible cases: biconical, conical-hemispherical, hemispherical-conical, and bihemispherical. [9, 10]

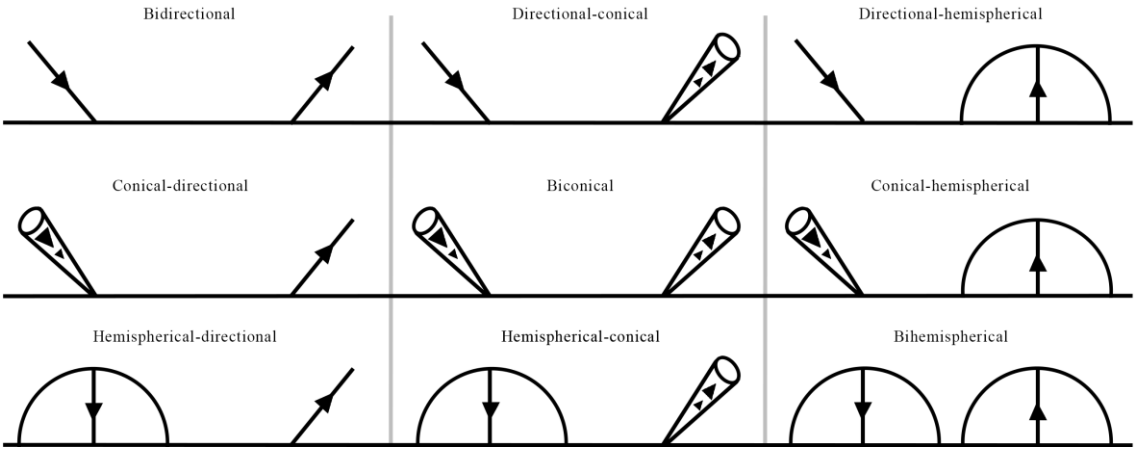

Figure 3. Nine geometric domains of incident radiance (down-arrow) and reflected radiance (up-arrow). Figure is an adaptation of a literature reference [10].

Spectral bidirectional reflectance factor, BRF_λ is defined in a given view direction as the measured spectral radiance from a target surface to the measured radiance of a reference standard surface under the same illumination and view conditions. The reference standard on to which the target radiance is compared to should resemble a lossless, ideally diffuse, perfect white surface referred to as Lambertian surface. A Lambertian surface has a constant radiance into any view angle (Figure 4). [9, 10]

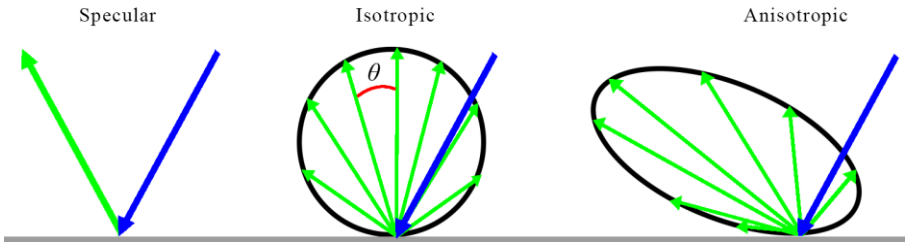

Figure 4. Radiance scattering geometries. Isotropic corresponds to the geometry definiens as a Lambertian surface. The radiance into zenith angle θ has a magnitude proportional to *cos(θ)*.

The mathematical definition of bidirectional reflectance factor [9] when using an ideal Lambertian surface as a reference standard and an illumination from a single direction is shown in Equation 3:

$$\mathrm{BRF}(\theta_i, \phi_i; \theta_r, \phi_r; \lambda) = \frac{L_{\mathrm{target}}(\theta_i, \phi_i; \theta_r, \phi_r; \lambda)}{L_{\mathrm{ref,ideal}}(\theta_i, \phi_i)}, \quad (3)$$

where L_{target} is the target radiance and $L_{\mathrm{ref,\ ideal}}$ the radiance from an ideal Lambertian reference panel, with both being functions of measurement geometry and wavelength. The directional angles for incident and reflected radiation are defined in Figure 5.

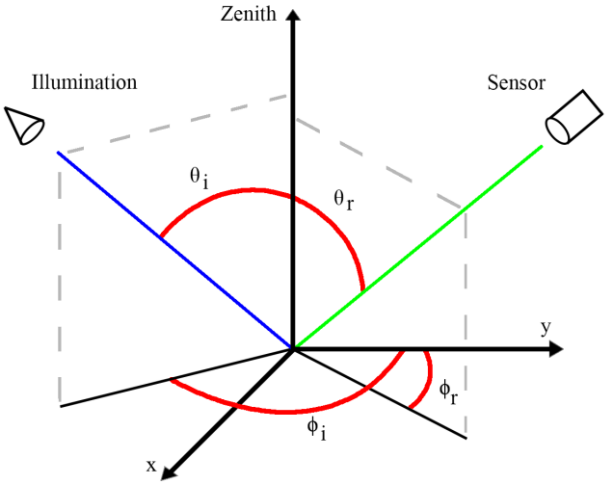

Figure 5. Measurement geometry defined in spherical coordinate system. Directions of illumination (blue) and sensor (green) as functions of zenith angles θ_i and θ_r (red), and relative azimuth angles ϕ_i and ϕ_r (red). Compass pointing of y-axis can be chosen freely but the direction should be unambiguous, e.g. north or the direction of the illumination.

Manufacturers that produce the white reference panels used in BRF measurements aim to refine their products to mimic the optical properties of a Lambertian surface as close as possible. Panels like the industrial standard Spectralon® by Labsphere, used also in the measurements of this study, have a near-perfect nadir reflectance of 99% over the optical spectrum [11]. The deviation from ideal diffuse surface is corrected by adding a correction factor in the reflectance factor equation as in Equation 4. However, further

studies on spectralon anisotropy have shown that Spectralon® reflectance panel has as well an angular dependency [12] which should be included in the correction factor [13]. An extended version of Equation 3 for calculating BRF including the correction factor is shown in Equation 4:

$$\mathrm{BRF}_\lambda = \frac{L_{\mathrm{target}}(\theta_i, \phi_i; \theta_r, \phi_r; \lambda)}{L_{\mathrm{ref}}(\theta_i, \phi_i)} R_{\mathrm{ref}}(\theta_i, \phi_i; \theta_r, \phi_r; \lambda)\,, \tag{4}$$

where L_{target} is as previously, L_{ref} the measured radiance from the non-ideal reference panel, and R_{ref} the known reflectance factor of the panel added for correcting BRF for angular and spectral dependencies.

BRF is a simplified quantity since it is an average over the designated solid angles in both illumination and viewing geometries. A more complete description of a target's reflectance properties and a definition for the directional reflectance for all possible illumination and view angles in the hemisphere is given by the bidirectional reflectance distribution function (BRDF). Because BRDF considers infinitesimal solid angles of both the spectral directional radiance leaving the surface, and the spectral directional irradiance arriving on the surface, it is not a measurable quantity as such but is replaced by BRF in measurements. The relation between BRF and BRDF arises from the characteristic diffuse reflection property of the Lambertian surface, resulting the same radiance to be reflected into all view directions. BRDF of an ideal Lambertian surface is $1/\pi$ and is defined as in Equation 5 [9]:

$$\mathrm{BRDF}_\lambda(\theta_i, \phi_i; \theta_r, \phi_r; \lambda) = \frac{dL_r(\theta_i, \phi_i; \theta_r, \phi_r; \lambda)}{dE_i(\theta_i, \phi_i; \theta_r, \phi_r; \lambda)} = \frac{\mathrm{BRF}(\theta_i, \phi_i; \theta_r, \phi_r; \lambda)}{\pi}, \tag{5}$$

where dL_r is the radiance from the surface to an infinitesimal solid angle and dE_i the incident irradiance from an infinitesimal solid angle. The directional reflectance is defined by considering the level of collimation in both the incident illumination beam and the reflected beam.

2.3 Measuring bidirectional reflectance factor

Both BRF and BRDF are clearly defined as was shown in Equations 3, 4, and 5. Although BRDF is not measurable as such, it is pursued due to its non-integral-nature which allows quantification of point-like reflectance with directional and spectral dependencies.

In laboratory environment, given a well collimated illumination beam, a relatively small field-of-view of the sensor optics, and using a non-imaging spectrometer, the radiance measurements take place in a directional-conical measurement geometry. Additionally, if the measured surface is free of radical spectral anisotropic features, the theoretical directional measurements are averaged within the solid angle of the conical geometry. Spectral laboratory measurement techniques that include the represented constrains provide therefore well approximated measurements in bidirectional geometry domain. The bidirectional geometry was defined earlier in Equation 3 and 4. [13]

Obtaining BRF in outdoor environment is more challenging due to the diffuse sunlight conditions. However, these measurements can be made by collecting the radiance both

under hemispherical illumination geometry and under hemispherical geometry with the direct components removed by shadowing the target surface. This should be done both for the reference measurement and for the target measurement. The contribution of the directional component can be later resolved by substracting the obtained spectral radiance from each other. [13]

As stated, spectral measurements made in field conditions under natural solar illumination require a lot of ancillary data to be collected compared to laboratory measurements. Data on diffuse sky and clouds, wind, shadowing of trees and other obscuring elements, reflections from the environment, and the role the time of day play on these should be known. The conditions should be constantly monitored, and changes noted. This is especially important if a single reference measurement is used for determining reflectance factors of multiple successive target measurements [14]. Additionally, having knowledge of the preceding precipitation is also important due to strong spectral absorptive property of water. [8]

Calculating the bidirectional reflectance factor from the measured radiance is relatively simple as was shown in Chapter 2.2. However, having truly meaningful results depend heavily on the suitability of the measurement instrument for a given target, on the information available on the prevailing measurement conditions throughout the data collection period, and on the expertise of the operator and his/her abilities to use the equipment and to monitor the data collection process. In the laboratory, the conditions related to the illumination, target topography and geometry, and the radiation environment can be considered stable and therefore laboratory measurements are easier to control. The following assumptions should be related to any BRF measurements regardless of equipment or measurement environment [15]:

1. The sensor field-of-view is limited to 20°.

2. The white reference panel surface area covers the sensor footprint area in full.

3. The irradiance falling on the sensor footprint remain constant between the white reference standard radiance measurement and the target radiance measurement.

4. The sensor electronics have a linear response for changes in radiant flux.

5. The reflectance properties of the white reference standard are known in the given illumination and view geometry.

The sensor field-of-view is limited to ensure measurements from a relatively small irradiated area on the target. This enables attaining the directional nature of the radiant flux leaving the projected source area in a solid angle into the direction of the sensor.

2.4 Physical basis of multiangular observations

A basic illustration of a single scattering model for evaluating the reflectance of two-layered vegetation structure of canopy and soil is shown in Figure 6. For a given set of view and illumination angles, the sensor sees different amount of canopy and soil as partly illuminated and partly shaded. The recorded radiant energy by the sensor is therefore strongly dependent on the illumination and view geometries. In general, the parts of the

canopy and underlying soil that are under direct illumination appear brighter to the observer than the parts that are in shade. From the nadir view directly above the scene, the sensor has the largest amount of soil visible due to the canopy gap fraction which has its largest value at that view direction. The soil can be either illuminated or shadowed which depends on the optical properties of the surrounding elements. Canopy gap fraction, and related view angle dependencies on the measured radiance, has been previously studied [16] with reported results supporting the significance of understory contribution to the overall radiance from nadir-view. As the view zenith angle is increased, the amount of soil in the field of view of the sensor gradually decrease until an angle is reached where only the forest canopy is visible to the sensor. This means that the spectral response of a forest canopy in a natural scene has a strong dependency on the view zenith angle. Canopy anisotropy can be related to understory vegetation where e.g. dwarf shrubs have their own canopy with an underlying vegetation and soil [17].

The single scattering model shown in Figure 6 can be used also to explain the so called hotspot effect which occurs when the illumination and the view angle have a phase difference of zero. In hotspot geometry the observer is located on an imaginary line connecting the target and the illumination source, pointing the spectroradiometer directly towards the target. In this geometry, all the scene elements in the field-of-view of the sensor are illuminated and the recorded radiance has a sharp peak representing its maximum value. The peak radiance is a consequence of maximum shadow-hiding, a phenomenon which can be explained by considering radiation field with relatively short wavelength incident on a larger size scatterers. This generates shadows but at the hotspot direction these shadows are hidden by the objects themselves that generated the shadows, thus generating fully illuminated field-of-view. The shadow-hiding is noticeable in reflectance anisotropy measurements of relatively heterogenous surfaces on the principal plane at view zenith angles approaching the illumination direction. The hotspot effect is further strengthened by so called coherent backscatter effect which deals with adding of phases of photons in a scattering medium resulting amplification of the backscattering signal. Some natural scene elements, such as still water bodies and waxy flat leaves have a strong anisotropic reflectance characteristic also into the forward direction, the direction exactly opposite from the direction of the illumination on the principal plane. [18,19]

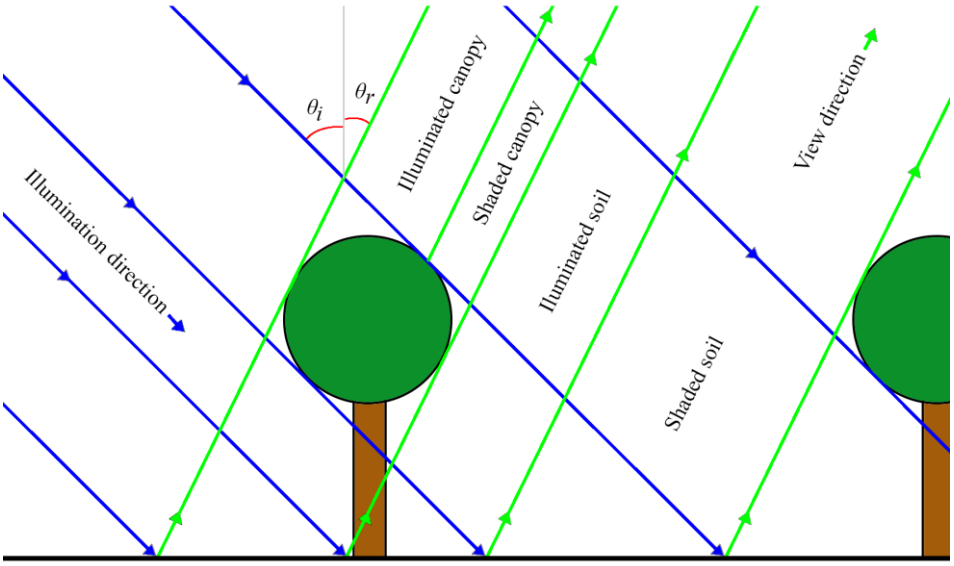

Figure 6. Single scattering model of an incident radiation field on a two-layered vegetation structure. Figure is an adaptation of a literature reference [20].

2.5 Instruments for measuring BRF

Terrestrial multiangular BRF measurements typically utilize a traditional goniometer design. In this design the sensor optics are rotated around the sample both in zenith and in azimuth directions (Figure 7). The illumination can be either natural sunlight when measuring outside, or originate from an artificial illumination source (a lamp) in laboratory measurements.

Multidirectional reflectance measurements provide empirical radiometric information on target surface anisotropy. The spectral anisotropy can be evaluated by measuring the energy in the reflected fraction of the incident energy which originates from a given direction and scatters from the target surface towards the sensor. Over the course of past 30 years, several research institutes and companies have developed instruments for measuring spectral multiangular BRF of different target types, in different environments and in different scales. Spaceborne instruments such as MISR (Multi-angle Imaging SpectroRadiometer) on-board NASA's Terra-satellite, or CHRIS (Compact High Resolution Imaging Spectrometer) on-board European Space Agency's PROBA-1 (Project for Onboard Autonomy) satellite provides comparable reflectance anisotropy information to data obtained using a field goniospectrometer, such as FIGIFIGO. Satellite data is used to derive global products like leaf area index (LAI) or planet albedo, while field instruments measure ground truth reference data for calibrating satellite instruments and validating mathematical scattering models.

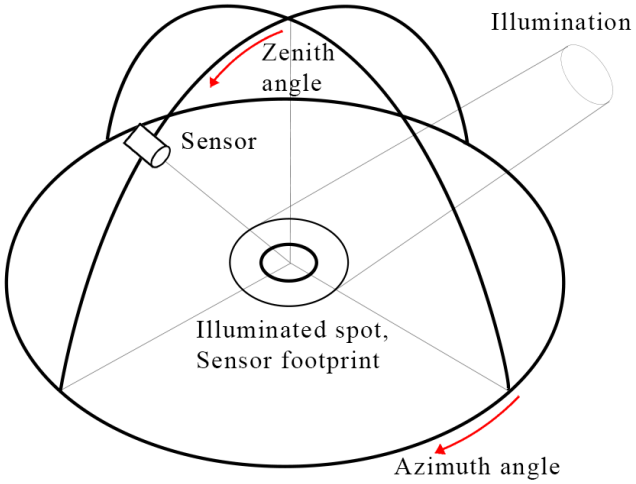

Figure 7. A wire-model of a traditional spectral goniometer design. The illumination source produces a collimated beam of light towards the illuminated spot. The sensor measures the spectral radiance leaving the illuminated spot towards the sensor.

2.5.1 Field and laboratory goniospectrometers

In addition to FGI's FIGIFIGO, several other field goniometer systems have been developed by other research institutes. Possibly the most famous FIGIFIGO preceding field capable system is Field-Goniometer System (FIGOS) built at the University of Zurich in 1994. FIGOS represents a traditional goniometer viewing geometry and structure design. A rigid support structure has a 2 m radius half-arc (zenith arc) going over the sample area enabling the sensor positioning in zenith direction. In azimuth a

horizontally oriented full-circle (azimuth rail) allows the rotation around the pivot point at the centre of the local spherical coordinate system. The operation is semi-automated: a motor driven sled carrying the sensor optics moves in zenith direction while manual labour is required for azimuthal rotation of the instrument. [21]

Another famous goniometer was introduced in 1994 by Join Research Center of the Commission of the European Union: European Optical Goniometric Facility (EGO), a fully automated laboratory goniometer. As a stationary system EGO has a more robust 2 m radius structure compared to FIGOS. The goniometer is contained inside a special black walled laboratory. [22]

The first automated field goniometer was the Sandmeier Field Goniometer (SFG), a laptop controlled version of FIGOS, constructed for NASA in 1999. In SFG any sensor position within the hemisphere can be achieved automatically. Hemispherical BRDF is achievable in 10 minutes with 15° and 30° angular resolutions in zenith and azimuth direction respectively. The structural dimensions of SFG match those of the FIGOS. [23]

The Portable Apparatus for Rapid Acquisition of Bidirectional Observation of the Land and Atmosphere III (PARABOLA III) represents a different approach in measuring surface anisotropy: it applies a viewing geometry directed outwards from a fixed position at the centre of a local spherical coordinate system. This is opposite to the traditional way where the viewing is from a fixed radius inward to the origin of the coordinate system. PARABOLA III is a custom instrument built by Sensit Technologies Inc. in 1998. The goniometer geometry enables angular measurement of both incident hemispherical irradiance and the radiance leaving the surface. The instrument has been used to collected reference data for the spaceborne MISR instrument. Due to its viewing geometry and varying location of the field-of-view of the sensor, the measurable target types are limited to homogenous surfaces. [24]

Automated Spectro-Goniometer (ASG) is a compact fully automated goniometer for field measurements developed at the University of California, Santa Barbara in 2003. The instrument was developed for snow and other smooth surface reflectance measurements in hemispherical-directional geometry. The system is considerably light (49 kg) compared to FIGOS (250 kg) due to innovative automated processes and mechanical design. Compared traditional goniometers, the fore-optics have a small hemispherical radius around the target of 0.65 m. [25]

Another compact goniometer was developed at the University of Lethbridge in 2006. University of Lethbridge Goniometer System (ULGS) is a manually operated goniometer for field and laboratory use. One of the driving design objectives of the project was to develop a compact goniometer with traditional structure (half-arc and full-circle) but with a low price point. The affordability was to allow more users to access angular remote sensing measurements for resolving BRDF related problems. [26]

A new innovative way of utilizing an industrial robot for BRDF measurements was realized at Wageningen University on 2012. This design is a fully robotic laboratory goniometer system for measuring anisotropic reflectance and emittance of small size samples of patches of grass or soil. The hemispherical viewing geometry is accomplished by implementing a six-axis robot arm, carrying both a spectrometer with associated fore optics along with a thermal camera. The advantage of a fully automatic robot system is speed, angular resolution and directional accuracy. [27]

One of the most advanced recently published spectral goniometers is the Goniometer of the Rochester Institute of Technology-two (GRIT-T). GRIT-T works both in laboratory and in field conditions, implementing a setup of dual spectrometers: one for measuring the upwelling radiance and a second spectrometer for measuring the downwelling

radiance. The goniometer has high directional accuracy, is fully automatized and has innovative technology to reduce the wandering of the measurement spot, for mitigating self-shadowing of the sensor, and to enable self-levelling by utilizing inclinometers and related actuators. [28]

2.5.2 Airborne multiangular spectroscopy

The advance of aerial remote sensing techniques comes from the altitude and movement of the platform. Several applications from environmental monitoring to natural disaster response systems depend on the access to multi- or hyperspectral data. This data is required to have high spatial and temporal resolution, and large enough local geographical coverage. Addition to direct use, aerially collected spectral data have been also used to test, validate, and calibrate spaceborne instruments before and after launch. The designs of the systems vary depending on whether the airborne systems are designed to produce multi- or hyperspectral data, and if the data collection is made only from nadir view or by applying multiangular data acquisition.

AirMISR (Airborne Multi-angle Imaging SpectroRadiometer) was an aerial instrument designed to produce multiangular spectral data by utilizing a single camera on a controllable gimbal mount. The imaging spectrometer produced data in four spectral bands and at nine view angles matching those of MISR, the spaceborne counterpart of AirMISR. AirMISR was applied for providing reference data for MISR for sensitivity analysis and calibration. On the reference data acquisition missions, a NASA fixed-wind pressurized aircraft ER-2 was flown at high altitude of 20 000 m matching the path of the satellite carrying the MISR instrument. By having data collected in the same atmospheric conditions and illumination conditions AirMISR data acted as a comparative reference for MISR. [29]

OSIRIS, is a multi-viewing multispectral instrument used in BRDF studies from aerial platforms. Like AirMISR, also OSIRIS concept is based on a spaceborne POLDER (POLarization and Directionality of the Earth's Reflectances) instrument. Along with the wide field-of-view spectral imaging capabilities, OSIRIS has a polarizing wheel at -60°, 0°, and +60°. Polarizing wheel is used to study the polarization properties of surfaces, such as snow [30]. [31]

AirMISP (Airborne Multi-angle SpectroPolarimeter Imager) is a similar gimbal oriented system as AirMISR but an additional capability of doing polarimetric measurements. The instrument sensor has eight spectral bands in the optical region that record the radiance with a pushbroom acquisition technique, instantaneously measuring the response from a cross directional row of pixels and utilizing the along-track movement of the platform to generate an image. The research purpose of AirMISP is in atmospheric sciences, such as determining sizes of aerosol particles and optical depth. [32]

Unmanned aerial vehicles (UAVs) have an exciting potential to provide cost efficient localized aerial reflectance data with high temporal resolution and minimal delay. The prices of capable UAVs are already at consumer level and are being widely utilized in scientific studies for evaluating vegetation anisotropy [33]. Larger customized UAVs can carry more load and thus have improved control of stability, provide more accurate angular and location information, and in general carry heavier equipment, such as larger batteries or instruments such as laser scanners or hyperspectral cameras [34].

The concept of using a normal camera as a multiangular instrument is based on wide angle lens with a perspective change towards the edges of the image. As the UAV is flown

over the target area, the images acquired can be processed for multi-angular single target reflectance data. Imaging hyperspectral spectrometers can similarly produce multiangular datasets but with each pixel associated with its own hyperspectral data. This forms so called datacubes of the scene. [35].

2.5.3 Spaceborne multiangular spectroscopy

Only a few spaceborne instruments have been designed to produce multiangular reflectance data as their main function. Due to the large distance to the target, the varying view geometry can be achieved in different ways. One approach is to have a multiple angularly adjusted pushbroom cameras, such as in MISR, each of which constantly measure the radiance from the whole swath width and utilizes the satellite movement along the orbital track for generating an image [36]. A second approach is to have a single nadir pointing camera on board pointable satellite, such as the CHRIS, where the satellite orientation can be accurately controlled, and a chosen target imaged from several zenith angles [37]. A third method is to have a wide-angle imaging radiometer like the POLDER, where the image perspective changes sufficiently towards the edges of the image to enable collection of multiangular data [38]. It should be noted that due to differences in implemented technologies and purpose in data product usage, the swath-width, spatial resolution and spectral resolution of the satellite sensors differ greatly; the spatial resolution for nadir CHRIS image is 18m (or 36 m), MISR image 250m and for POLDER image several kilometres.

Because of the relatively large spatial resolution, spectral mixing is always a problem with satellite earth observation data, and typically reference data in form of ground truth are needed for calibration of the satellite instrument, for validating the data, and for improving the interpretation made from the data. Together with instruments of moderate and high spatial resolution, like MODIS (Moderate Resolution Imaging Spectroradiometer) on-board Terra satellite, or MSI (MultiSpectral Instrument) on-board ESA's Sentinel-2 satellite, global products such as hemispherical albedo and leaf area index can be derived, making spaceborne earth observation instruments vital for understanding environmental phenomena at global level.

3 Materials and Methods

3.1 Study area

The primary study area located in Masala, Kirkkonummi, Finland (coordinates 60.161˚N, 24.545˚E) on the premises of Finnish Geospatial Research Institute (Figure 8). The vegetation grew on top of a partly exposed bedrock with a sparse tree trunk density and low understory. The total planar area of the bedrock was approximated to be 14400 m^2 with elevation from sea level peaking at 34 m. Altogether three data collection sites were selected on the south- and southwest-facing slopes of the bedrock to have a representative collection of samples.

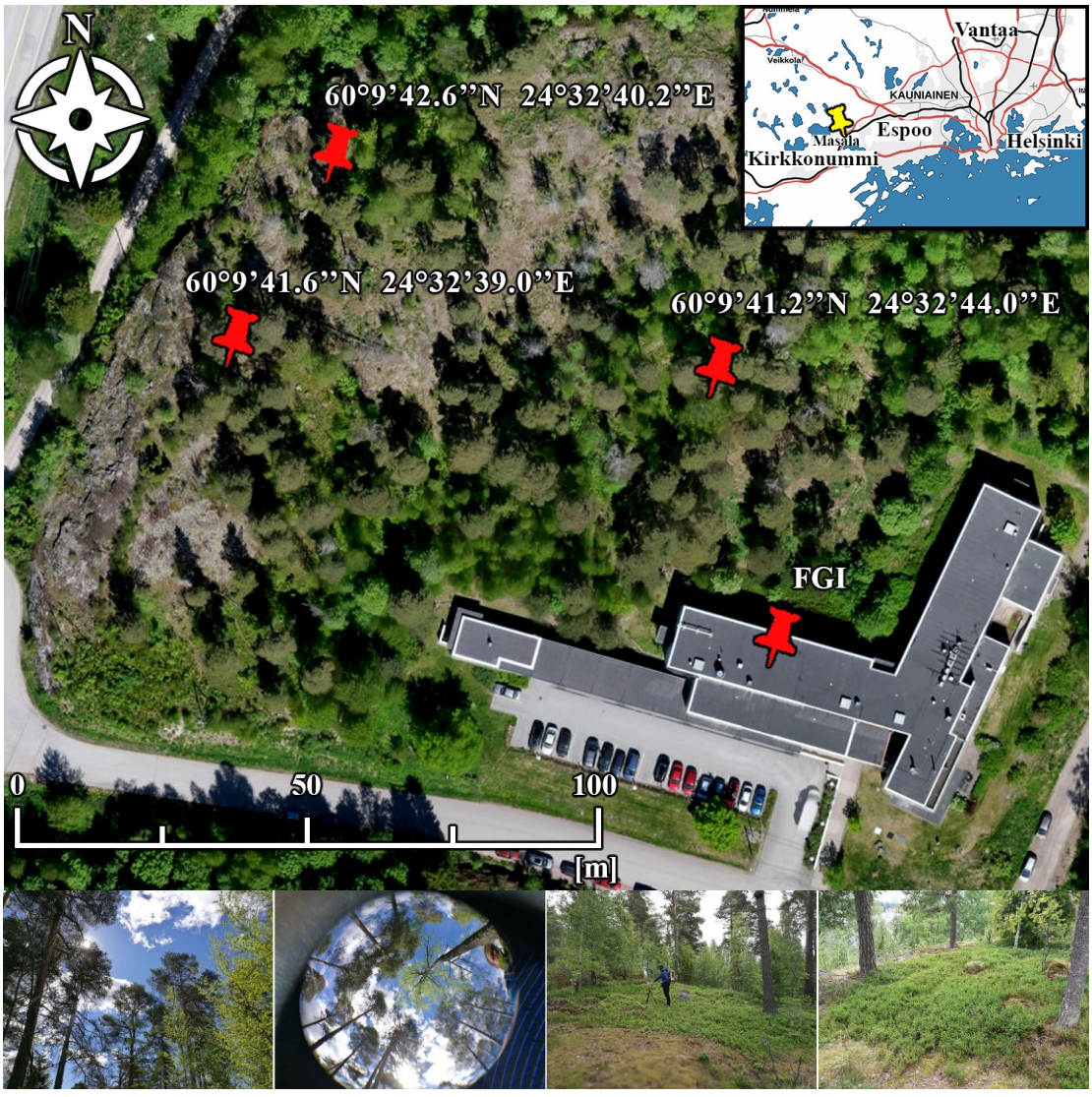

Figure 8. An orthophoto of the primary study area in Masala. The three sample collection sites and FGI headquarters are indicated by the red stamp icons. The orthophoto was generated through photogrammetric processing of several nadir photographs taken on 24 May 2016 using FGI’s drone. The image processed was done by Roope Näsi from FGI. The four smaller photographs at the bottoms show the typical tree species and dwarf shrub populations found at the data collection sites.

Before the sample collection, each site (Figure 8) was evaluated for the dwarf shrub species population density, for suitability considering available resources for sample digging and transportation, and for issues related to land management permissions. Typical boreal forest tree species and trunk density variation followed the soil thickness on top the bedrock which was thinner and drier at higher elevation. The forest type of the three sites was visually categorized using literature examples [39, 40] as sub-xeric, a class of dryish land forest with periodically moist soil from which water is removed rapidly after precipitation. At lower elevation the thicker soil layer supported mainly thin-leaved deciduous trees such as birches (*Betula pendula*), aspens (*Populus tremula*), and evergreen tree species such as Norway spruces (*Picea abies*) and Scots pines (*Pinus sylvestris*). In the higher elevation most of the sparsely growing trees were pines with a small number of junipers and young birches around the data collection sites. Similar variation was noted on the understory species. At lower elevation plants such as ferns and tree saplings flourished under deciduous canopy cover while at higher elevation mosses, lichen and dwarf shrubs were more common around pines.

A second study area used for measuring single leaf optical properties located at Aalto University campus in Otaniemi, Espoo, Finland (coordinates 60.191˚N, 24.831˚E). The sample collection site was a small forest area approximately 500 m from the spectral laboratory where the leaves were measured. The forest type differed from that located at Masala having more moist soil with dense populations of ferns and grasses, and more shadowed forest floor due to denser canopy cover consisting mainly of spruces (Figure 9). The largest contributing factors to the differences were the study area's closeness to a water body (<100 m), topographical flatness and low elevation (~7 m) from the sea surface. Both dwarf shrub species were found within 20 m distance from the given coordinates. Blueberry population was considered abundant relative to the lingonberry which was more difficult to locate. Following the same categorizing as previously, Otaniemi study area was categorized as mesic, a vegetated area where the underlying soil is adequate moist throughout.

Figure 9. Two photographs taken from the secondary study area in Otaniemi showing the abundance of forest floor vegetation, the dominating tree species, and a population of blueberry shrubs. Both photos were taken on 14 August 2017.

3.2 Samples

3.2.1 Collection methods and description

Altogether 20 natural sample plots were measured for BRF anisotropy with FIGIFIGO between DOY (day of year) 144 (May 24th) and DOY 272 (September 29th) 2017 (Figure 10). The measured samples included 9 lingonberry shrubs and 11 blueberry shrubs. Additionally, berry samples were measured on DOY 230 and DOY 258, lingonberry flowers on DOY 165, and leaf level reflectance and transmittance data were collected on DOY 226 and DOY 261 on both species. All samples were considered to represent the natural phenological stage typical to those species at the time of measurement and therefore to qualify as an input data for the multitemporal analysis.

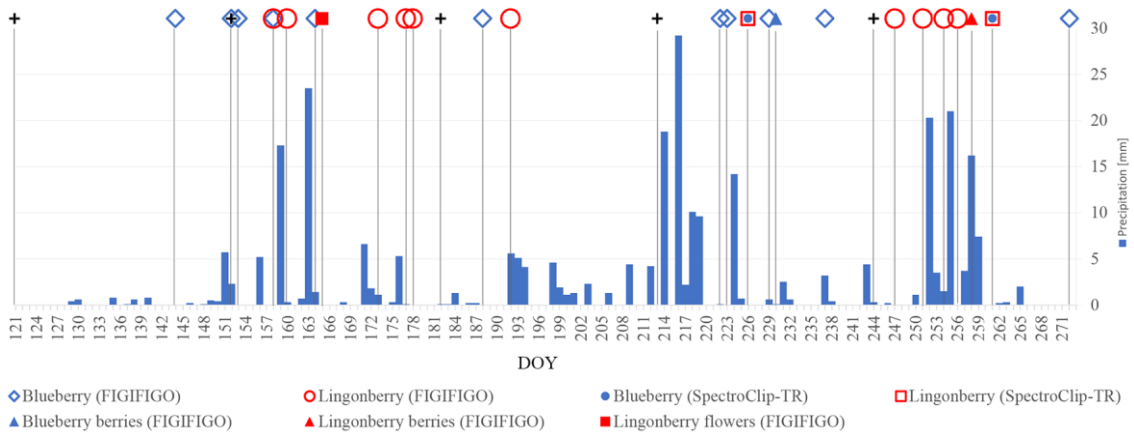

Figure 10. Timeline showing the day of year for each measurement and corresponding daily precipitation sum. The shown precipitation data is from an external source [41].

The BRF shrub samples were collected for measurements by digging the samples from the forest floor using a metal shovel and by transporting the samples into the spectral laboratory using a plastic sled. Before sample collection, each candidate plot was visually evaluated in nature for sample suitability to laboratory measurements using a set of questions that acted as a selection criterion:

- Is the dwarf shrub species present in the sample plots?
- Is the phenological stage of the shrubs in line with the expected?
- Is the dwarf shrub species the dominating species in the sample plot?
- Is the spatial distribution of the shrubs within the plot suitable for measurements?
- Is digging and transporting the sample possible using the methods available?
- Considering the surrounding environment, is the level of damage caused by the sample digging acceptable?

If a candidate sample met the given criteria, the sample was moved into the laboratory. On average the measured samples had the following dimensions: 0.7 m x 0.6 m x 0.4 m (Figure 11), where the first dimension is the cross-track dimension relative to the principal plane in the laboratory measurement geometry, the second one the along-track dimensions on the principal plane, and the third one the height of the sample from ground up to the top of the canopy including the underlying soil. All samples had 10 cm to 15 cm layer of soil and on average 30 cm tall dwarf shrubs population on top, resulting an overall height between 40 to 45 cm. Some degree of downward sloping was noticed towards the outer edges. This was caused by the shovel moulding the bottom side thinner at the edges compared to the centre of the sample.

Figure 11. Horizontal dimensions displayed on an average size dwarf shrub sample measured in this study.

All samples were removed from the ground along with thick rooted layer of soil. Any roots that reached deeper into the ground were cut using cutters or the tip of the shovel. The samples were then placed onto a plastic sled for transportation to the laboratory. Because the data collection sites were located on elevated bedrock, with steep slopes and boulders making the surface topographically uneven, special care was taken in keeping the structure of the samples as natural as possible during transportation with the sled.

At the laboratory entrance, before the sample was moved inside, the sample was lifted from the sled onto a dark plywood support plane which served as a sample holder during the following BRF measurements. The plywood plane, along with the sample was then carried inside the laboratory facilities and placed into the illumination spot and the sensor footprint.

The duration of the BRF sample collection from the beginning of digging to the beginning of the first measurement was on average 36 minutes, with occasional variations due to technical problems, typically related to the stability of the control software. The measurements themselves took on average 4 h per sample to complete and were mostly made between 10 AM and 2 PM local time. All samples were returned to their original collection locations after measurements.

On two separate dates during the research effort, ancillary spectral measurements were made for collecting single leaf reflectance and transmittance data of the two dwarf shrub species. The leaf samples were acquired from a forest next to the Aalto university facilities in Espoo. The university facilitated the spectral laboratory and the equipment

for the measurements. Due to challenges related to the transportation of the leaved dwarf shrubs in a natural state to the laboratory, an innovative approach was used: a tall plastic box with a 10 cm thick layer of moisturized soil at the bottom was used as a temporary habitat for the dwarf shrubs which were placed with full roots into the box immediately after collection. The box was then transported to the nearby laboratory and placed inside a pre-cooled refrigerator (dark, temperature ~ 5 ˚C) to limit the physiological changes. The leaf measurements were conducted between 9 AM and 4 PM local time and all together 117 leaves were measured.

3.2.2 Measured phenological stages

The study was timed to extend over most of the 2017 growing season in southern Finland. This ensured multitemporal data collection and thus spectral data on different phenological stages of the dwarf shrubs species. Statistically the growing season in southern Finland began on DOY 121 (1st May) and continued until DOY 291 (18th October). According to the heat sums recorded by the Finnish Meteorological Institute from the past three years, in 2017 the growing season in southern Finland (Helsinki region) begun somewhat later than on previous years (2014: DOY 107, 2015: DOY 98, 2016: DOY 119). When comparing to the recorded average of 1981 to 2010, in 2017 the growing season started approximately a week later. The first sample in this study was measured on DOY 144 (24th May) and the last on DOY 272 (29th September), resulting more than 75% temporal extend over the growing season. [42]

Four distinctive phenological stages were separated and were measured as applicable:

- Leaves-on.
- Flowers.
- Berries.
- Senescence.

The leaves-on stage represented the dwarf shrubs after leaf development (lingonberry is evergreen) without any flowers or berries, the flowers stage and berries stage referred to shrubs with flowers and berries respectively, and the senescence stage to the autumn samples measured in the end of the research effort. Addition to the four phenological stages, a soil stage was measured of each sample. The soil stage spectral reflectance factor was desired for determining its contributive effect on the dwarf shrub spectra and to observe potential phenological changes in the soil layer (Table 1)

Table 1. Measured phenological stages of each BRF sample. Indices B and L stand for blueberry and lingonberry respectively. The associate running number next to the index describes the temporal order in which the samples were measured. Samples with "pp" are measured only on principal plane. Two illumination zenith angles were applied in majority of measurements (+40°, +55°).

	Leaves-on		**Berries**		**Flowers**		**Soil**	
Index / θ_i [°]	+40	+55	+40	+55	+40	+55	+40	+55
Blueberry								
B_spring	x							
B1	x							
B2	x	x					x	x
B3	x(pp)	x(pp)					x	x
B4	x	x			x	x	x	x
B5	x	x					x	x
B6	x	x	x	x			x	x
B7	x	x	x	x			x	x
B8	x	x	x	x			x	x
B9	x	x	x	x			x	x
B_autumn	x	x					x	x
Lingonberry								
L1	x(pp)	x(pp)			x	x	x	x
L2	x	x					x	x
L3	x	x			x	x	x	x
L4	x	x			x	x	x	x
L5	x	x					x	x
L6	x	x	x	x			x	x
L7	x	x	x	x			x	x
L8	x	x	x	x			x	x
L9	x	x	x	x			x	x

The preparation of the dwarf shrub samples for the soil stage measurements included cutting away the shrubs, leaving the underlying material as such. The exposed soil consisted mainly of typical forest floor litter in form of dead tree leaves and dwarf shrub leaves, dry needles and grass, and small twigs. In minority was alive vegetation such as mosses and seasonal grasses.

Manipulation was also applied to samples in flowers and berries stages, where after the BRF measurements of their natural phenological stages, the flowers and berries were removed, and the samples were measured again, now as representatives of the leaves-on stage. This was done for two reasons: to increase the number of samples in the leaves-on stage, and to produce sample pairs for comparative analysis for detecting flowers and berries. Majority of the samples were measured using two distinct illumination zenith angles: +40˚ and +55˚.

Addition to the bidirectional reflectance factor measurements of the dwarf shrub and soil samples, and the leaf reflectance measurements, also the spectral responses of the berries of both species, and the flowers of lingonberry were measured (Figure 12). The measurements were made in FGI's spectral laboratory in Masala using the same laboratory setup as with the dwarf shrub samples. Both berries and flowers were picked by hand, lingonberries and flowers from Masala study area and blueberries from a

separate forest area in east-Vantaa (coordinates 60.270˚N, 25.086˚E). Lingonberries and lingonberry flowers were measured within 2.5 hours from the start of picking while blueberries were picked on the previous day of the measurements, kept in a refrigerator overnight in several small plastic boxes, and transported next day to Masala laboratory.

Figure 12. Photographs of BRF measurements of (a) lingonberry flowers, (b) lingonberries, and (c) blueberries at Masala spectral laboratory. The diameter of the shown sample support (ring shaped) is 30 cm and height 20 – 30 mm. Two red dots are laser pointers from FIGIFIGO optics marking the sensor footprint on the target.

3.3 Measurement methods

3.3.1 FIGIFIGO

The bidirectional reflectance factor measurements of the two dwarf shrubs species were carried out using the latest iteration of the Finnish Geodetic Institute Field Goniospectrometer. FIGIFIGO was developed at the FGI over the course of years from 2004 onwards [43], with further developments done in the consequent years [44]. The instrument has been actively used since its launch and has provided validated data for several scientific studies. FGI's measurement campaigns involving FIGIFIGO have included spectral measurements on materials such as snow [45], understory vegetation including lichen, moss, and dwarf shrubs [17], and asphalt [46]. The collected data has been used both as such for the study of reflectance properties of different surfaces, and as ground reference for airborne, UAV and satellite instruments.

The experiences from the previous measurement efforts, and from the measurements made during this study, have shown the success of the FIGIFIGO design which underlines light weight and compact structure. The laboratory setup of FIGIFIGO and the sample illumination principle is shown in Figure 13. At the basic level, the instrument is built-up of a set of changeable sensor optics set on top of a tilting carbon arm, drivable in different zenith angles by a central motor. The motor and data collection are controlled by a computer program from a separate laptop. The motor, the control electronics, the spectrometer, and in field configuration batteries, are all enclosed inside a plywood box which additionally acts as a pivot support to compensate for the unbalancing forces from the tilting of the arm. The sensor optics are orientated 90° relative to the arm with a rail system stretching outwards. The rail system allows the attachment of several vital components, such as the flat diagonal mirror to reflect and direct the up-dwelling radiance from the sample to a 45° angle into the sensor optics, a stray light blocker to reduce the

amount of light from the surrounding environment, and two laser pointers that mark the edged of the footprint on the sample.

The sensor optics collect the radiance from the sensor footprint of approximately 9 cm in diameter in front of the plywood case. An optical fibre cable is connected at the back of the optics and transmits the light to a spectrometer for decomposition to three different sensors and sampling. The spectrometer used was from Analytical Spectral Devices, Inc (ASD) FieldSpec Pro FR, measuring at wavelength range from 350 nm up to 2500 nm.

In laboratory configuration, FIGIFIGO instrument body lies on top of rigid steel ring with diameter of 2 m. The sample is placed in the centre of the ring and FIGIFIGO is rotated in azimuth by manually turning the ring. The ring design includes built-in roller wheels for accurate movement and an optical encoder which records the ring movement and relates the angular information with 1° accuracy [44].

During the laboratory measurements, the sample is illuminated by an artificial light source which in this study was a OSRAM 1000W tungsten halogen lamp with sanded surface to reduce shadowing of filament, Oriel/Newport power supply, and Oriel/Newport lamp housing. The beam geometry of the light is collimated by using an off-axis paraboloid mirror to collect and reflect the light to the sample area via a large flat mirror which is adjustable both in height, position, and tilt. The adjustability of the mirror allows setting the illumination zenith angle. FIGIFIGO includes several technical features for laboratory and field-use that are not described here due to relevance to the study. These features have been reported in detail by the instrument developers in several public reports [43, 44].

The operation of the goniometer is controlled through a GonioControl4-software, a custom built LabView based interface. All the various sensor outputs in the system are fed into the software which drives the arm and generates a structured data log of the measurement, including the data on illumination geometry and metadata.

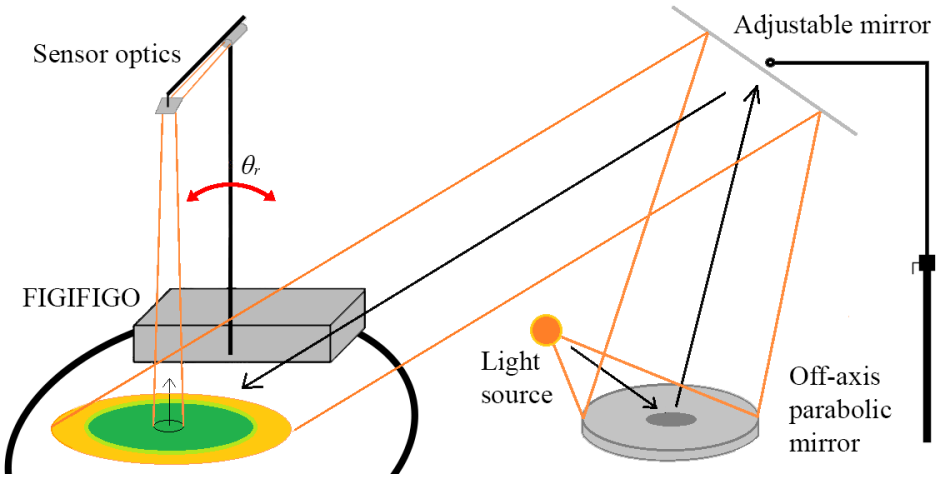

Figure 13. FIGIFIGO laboratory measurement setup and the applied illumination beam geometry. Figure is an adaptation of a literature reference [13].

The illumination and viewing directions were decided after assessing the constraining geometrics of the samples and FIGIFIGO structure. In laboratory setup, the pivot point of the tilting arm is at 14 cm from the ground, meaning that if the sample is a solid surface placed 14 cm from the ground up inside the measurement footprint, the only distortion to the footprint geometry is the elongation caused by the tilting of the arm. The elongation

of the footprint means the stretching of the longitudal diameter of the sensor footprint as the tilting arm is driven in larger zenith angles. This introduces an error source to the radiance measurements as the elements reflecting the incident radiation do not remain the same between different zenith angles. The basic relation of the sensor zenith angle and the footprint length is shown in Equation 6:

$$l = \frac{d}{\cos(\theta_r)}, \tag{6}$$

where l is the footprint length in longitudinal direction, d the diameter of the beam geometry, and $1/\cos(\theta_r)$ the elongation factor. A related error source to elongation is the movement of the centre of the sensor footprint relative to the nadir position. If the height of the sample exceeds the pivot point of the arm considerably, the footprint centre travels on the sample surface towards the sensor and vice versa. This is shown in Figure 14, where the centre location at 26° sensor zenith is compared to the centre location at 0°. As a result, and as was the case with elongation, the reflecting elements of the target are not the same at different sensor zenith angles if the difference between the angles is large. The sensor footprint can also partly, or completely, move outside top of the sample canopy if the sensor zenith angle is increased extensively, resulting measurements to be taken from the side of the sample instead of the top.

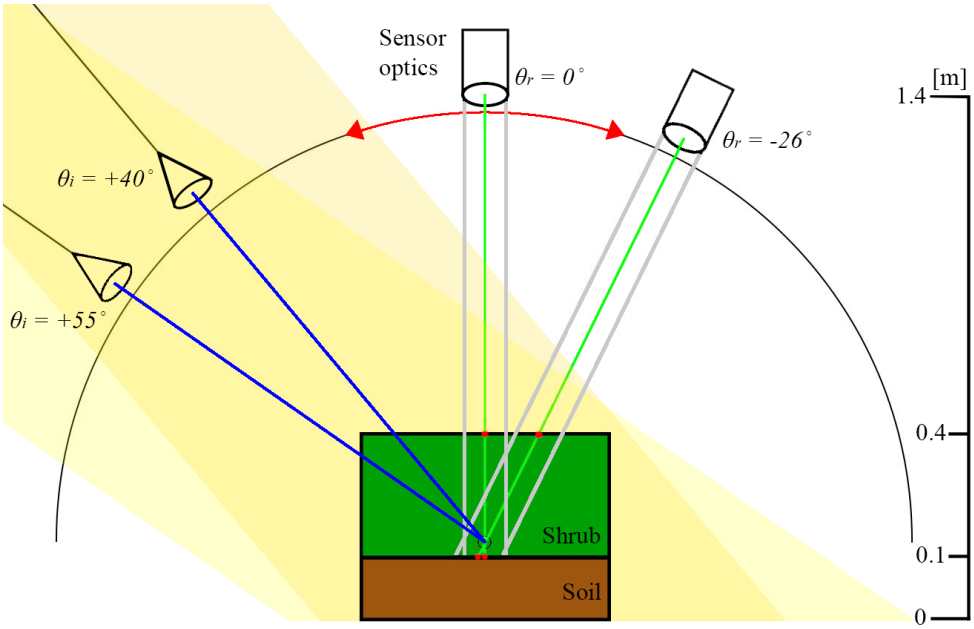

Figure 14. FIGIFIGO measurement geometry on the principal plane. The sensor optics are shown in two zenith angles as are the illuminating beams.

Determining the optical centre on which to evaluate the effects of these error sources is difficult in case of volume scatterers, such as the natural dwarf shrubs samples measured during this research effort. Therefore, following the measurement-, viewing-, and sample-geometries shown in Figure 14, sensor zenith angles of 26° and 40° were chosen as angles to represent the backward and forward viewing directions. At 26° angle, the sensor footprint elongates less than 12%, moves less than 13 cm from its nadir centre,

and avoids completely the self-shadowing of the arm structure in the hotspot direction. Additionally, 26° represents the off-nadir cameras of MISR instrument.

The BRF measurements of the dwarf shrubs were made using two distinct illumination zenith angles that correspond to the solar zenith angles at the given latitudes from May to August (Figure 15). Typical spectral field measurements take place in a constantly varying illumination geometry, and thus having a ground truth data collected in more than one illumination zenith angle furthers the usefulness and value of those data. Air- and spaceborne data acquisitions are similarly affected by the reflectance anisotropy. Being commonly utilized in large-scale multitemporal research of land covers, air- and spaceborne systems are expected to benefit from ground truth data which quantifies the spectral effects of the changing solar zenith.

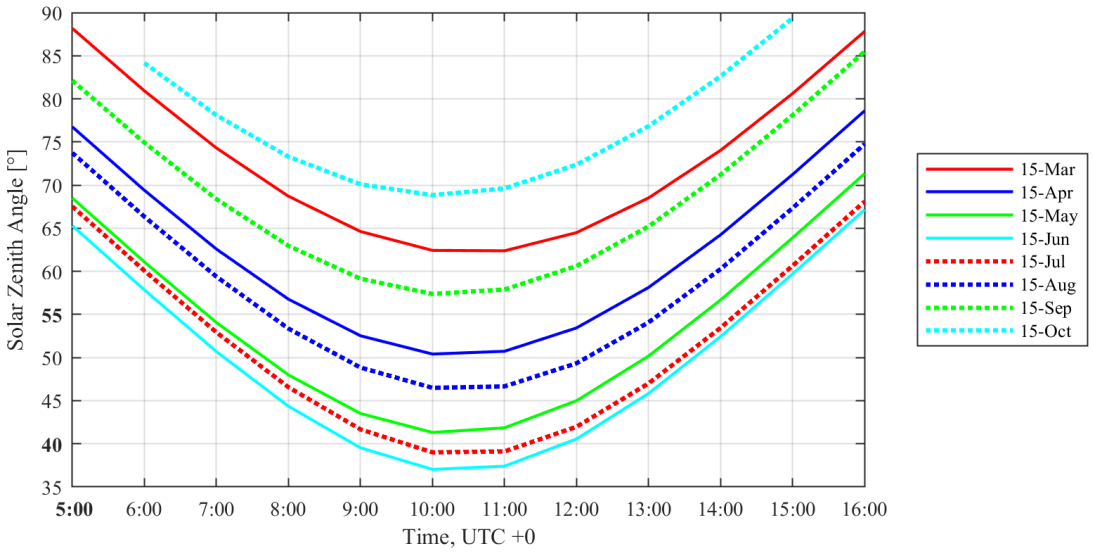

Figure 15. Annual sun path from 15th of March to 15th of October in one-month intervals at Masala study area coordinates. The time standard of the data is UTC (+0); Finland is in UTC+2. Solar zeniths 40° and 55° on y-axis refer to the two illumination angles used in the BRF measurements of this study. Data are from an external source [47].

Multiangular goniometer BRF measurements produce large amount of spectral data. The obtained data should be visualized for purposes of validating the success of the data collection. In the analysis it should be possible to re-structure the data to meet the purpose, e.g. for assessing of the anisotropy and optical properties of the target. Each bidirectional reflectance factor measurement produces a multi-dimensional feature vector exceeding the dimensions of 3D- feature space, thus making the data as such challenging to visualize. One way to solve the problem is by selecting only a single wavelength to visualize, and by plotting the reflectance factor in that wavelength as a function of the viewing and illumination angles. This produces a wavelength dependent point cloud, referred here as a BRF surface. The readability of the surface figure can be further improved by assuming left-right-symmetry of the sample, meaning that the sample is assumed to have symmetrical halves occupying different sides of the principal plane and thus, enabling splitting of the surface in half on the principal plane. This kind of semi-circle reflectance surface is given as an example in Figure 16.

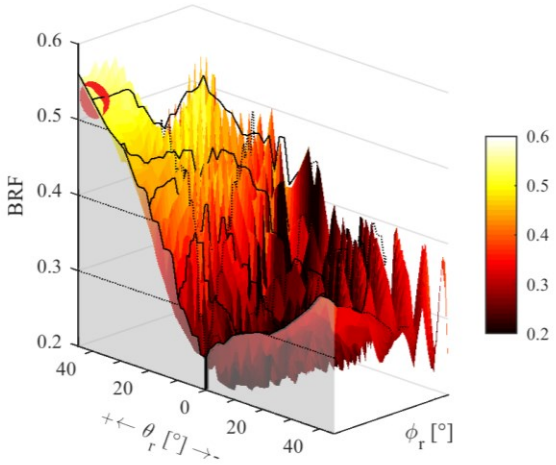

Figure 16. A semi-circle BRF surface plot commonly used for visualizing multidirectional BRF data. The red dot on the BRF-axis mark the location of the illumination source and θ_r-axis is on the principal plane. The data are examples of those measured from lingonberry shrubs.

When measuring targets with considerable structural and spatial heterogeneity, the smoothness and stability of the resulting BRF surface is determined by the optical properties of the target, spectral properties of the sensor, sensor optics, sensor movement, and the level of collimation of the illumination [44]:

- Sensor and sensor optics determine the spectral linearity and the evenness of the optics field of view.
- Sensor movement and related technical solutions determine the angular resolution and thus the density of the point set.
- The quality of collimation of the illumination radiation field affects the measured radiance if the measurement location varies between times of measurement.

If the sensor field-of-view is small and has high angular resolution, and if the surface composes of is spectrally rough scatterers, or contains varying shadows, the resulting spectral BRF surface can have noise-like characteristics. This characteristic noise from changing shadows and changing of contributing scattering elements in the sensor footprint during the angular measurement was shown in Figure 16 as an example of BRF data visualization. Although this noise can in fact be an accurate angular representation of the surface reflectance for measured sample area, as such it might make interpretation of the data more difficult. A smoothing function can be applied to the measured point set to generate a simplified model. Smoothing functions can be simple averaging functions acting on the neighbouring points or have included more complexity, such as weighting or assumptions of the expected anisotropy of the target.

In this study, all the spectra extracted from the obtained BRF datasets were smoothed using the second order Savitzky-Golay filter [48] with a 31nm window. The filter is included in Matlab as a function. Savitzky-Golay filter segments the data and filters the

segments for any sudden changes by applying polynomial fitting. The resulting spectra are a well tracking trend of the original data with increased signal-to-noise ratio.

FIGIFIGO raw data was pre-processed for BRFs using a selection of processing codes included in the FGI Reflectance Toolbox v1.1 [49]. The toolbox is written for Matlab and includes tools for loading the raw HDF5 (Hierarchical Data Format) structured radiance data in and calculating BRFs. The toolbox includes also various scripts for generating different graphical representations of the spectral data. Given the correctly structured input data, (1) the pre-processing begins by arranging and filtering the raw data points. The raw data and associated attributes along with the metadata are loaded into Matlab. (2) The data are converted into a structure where the measured spectra, white references, possible diffuse measurements, info, and the record log are grouped individually. Measured spectra are stored in sub-groups with timing and measurement geometry information. (3) The dark current is substracted from each measured spectrum already in the importing phase of the spectral data to remove the effect of the electric current induced by thermal fluctuations, a physical property of photoelectric sensors. (4) The operator then chooses measurement specific environmental parameters, such as the type of light source and sensor optics. (5) A manual filtering is suggested by the software in which the operator can remove specific measurements from the data set. This is to allow the user to remove the data collected directly inside the self-shadowing geometry. (6) Linear interpolation is applied for the white reference spectra to obtain reference values for each time of measurement. Because the white reference panel is a non-ideal Lambertian surface, the measure radiance from the reference panel is corrected for spectral and illumination direction dependencies by applying a correction spectrum to each measurement. (7) Reflectance factors are then calculated for each measurement location by dividing the measured radiance with the interpolated value of the white reference. The resulting spectral reflectance factor with associated directional dependencies and correction term was previously shown in Chapter 2.2 as Equation 4.

3.3.2 SpectroClip-TR

SpectroClip-TR (Figure 17) was chosen as a method for collecting leaf reflectance and transmittance data of the two dwarf shrub species. Leaf level spectral measurements lack the 3D-structure and therefore the within-canopy scattering, thus representing purely the surface and internal scattering properties of the leaf. Combining the leaf reflectance data with the BRF data collected from the shrubs in difference phenological stages, and of soil, enabled estimation of the contributive effects of individual scattering elements: leaves, berries, flowers, and soil. The SpectroClip-TR instrument, along with the associated equipment and spectral laboratory facilities were provided by Aalto University, where the instrument had been thoroughly tested and validated for operability in several preceding research efforts [50, 51, 52].

SpectroClip-TR is a double integrating sphere from Ocean Optics. When coupled with an external light source and a spectrometer, SpectroClip-TR can be used for measuring non-destructively both the reflectance and the transmittance spectra from the same spot on the leaf. The sample is held firmly between the two integrating spheres by a spring-loaded clip system that minimises undulation of the leaf surface at the sample port. Additionally, the firm grip and material choices reduce the amount of stray light from entering the spheres from the surrounding environment. Both spheres integrate the radiant flux from the sample, thus providing a reflectance and transmittance spectra in a

directional-hemispherical measurement geometry where the target is illuminated from a direction close to the normal of the leaf surface. Integrating spheres provide an enclosed measurement environment where the illumination conditions can be standardized. Since conditions inside the sphere are stable, and therefore same between each measurement, any recorded differences in the spectral responses can be assumed to be caused solely by the differences in the optical properties of the samples. The optical and structural properties can be further analysed for biophysical information, used in parametrization of radiative transfer models, or as a reference data as such for air- and satellite-imagery.

It should be noted that this quantity is different from bidirectional reflectance factor and therefore not directly comparable with FIGIFIGO measurements as such. The utilised 20 W light source was as well manufactured by Ocean Optics and an ASD FieldSpec4 Standard-Res was used as a spectrometer.

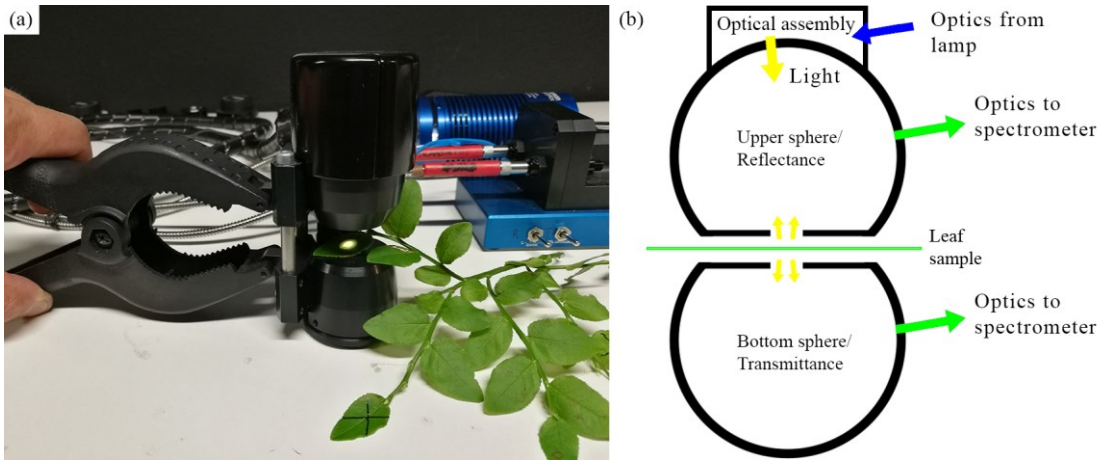

Figure 17. SpectroClip-TR, a double integrating sphere probe for measuring leaf reflectance and transmittance spectra. (a) A photograph showing the instrument in measurement configuration with jaws open, and (b) a concept diagram of a double integrating sphere probe. Figure (b) is an adaptation of a literature reference [52].

3.3.3 Measurement protocols

The process of collecting empirical evidence for scientific studies should include taking care of the traceability of measurement methods. This can be done by applying a tailored measurement protocols for each measurement method, and by following the protocols with minimum deviation throughout the research effort (Table 2). Consecutive measurements are typically required to be intercomparable, and enable validation and error analysis. Thus, applying a measurement protocol ensures that the data which are compared were obtained in the same way and in the same conditions.

The protocols that were followed in the measurements of this research effort differed between the devices due to differences in design and size. Also, it should be noted that the measurable quantities are different: FIGIFIGO measured reflectance factor whereas SpectroClip-TR is a double-integrating sphere-probe for measuring reflectance and transmittance. Both protocols included similar lamp and spectrometer warm-up times which were timed from so called cold-start to the beginning of the first measurement. The warm-up times ranged from 40 to 60 minutes which were considered adequate to achieve the operation temperature of the equipment required for normalized thermal conditions.

In FIGIFIGO measurement protocol (Table 2) the same sample was measured using two illumination zenith angles (+40°, +55°), resulting in repeating the protocol twice for each measured phenological stage and soil sample. Assuming stability of the illumination and the scattering environment in the laboratory environment, the white reference spectra was measured only in the beginning and at the end of each sample measurement. The basic structure of the protocol is represented previously in relation with studies using FIGIFIGO [13]. Spectralon® panel, manufactured by Labsphere Inc with dimensions 25 x 25 cm, was used as a reference panel in FIGIFIGO measurements to record reference radiance from nadir view. The panel is made of a PTFE (Polytetrafluoroethylene) with surface reflectance properties resembling those of an idea Lambertian surface over the optical spectrum. Fulfilling the diffuse prerequisite set for the reference panel in the BRF definition, Spectralon® panels are commonly used is spectral BRF measurements. Before each optimization and reference measurement, the white reference panel was centred inside the sensor footprint using the laser dot from FIGIFIGO, and carefully levelled using an integrated bubble level on the panel structure. Because BRF is calculated as the ratio of radiance from the surface to radiance from the reference panel, it is important to have the reference panel clean and levelled to avoid erroneous result. Impurities were removed from the panel surface several times during the study, both by cleaning the panel with sand paper under running water as instructed by the manufacturer, and by applying pressurised air to the panel between measurements.

SpectroClip-TR measurement protocol followed those of previous studies involving the same probe [50, 51]. The protocol includes “empty sphere”-measurement which are directly linked to the physics of integrating spheres. Physical background of double integrating spheres and theoretical calculations of reflectance and transmittance spectra from the measurements have been reported and validated previously by others [52]. The derivations of reflectance and transmittance from the raw data were applied as such in Matlab. SpectroClip-TR was used to collect reflectance and transmittance spectra from both sides of the leaves. These data are needed to describe the optical properties of the leaves. Additionally, the obtained data can be used as input for physically-based canopy radiation budget equations which model the scattering of the photons within the canopy structure [53]. In this study the obtained reflectance spectra are used to resolve contributions of different scattering elements in the dwarf shrubs. For SpectroClip-TR, a round, uncalibrated 1” (2.54 cm) diameter Spectralon® white reference panel was used. Similarly, as during the FIGIFIGO measurements, the surface of the panel was prepared following the manufacturer’s instructions and was kept clean between the measurements by applying pressurized air to remove any loose impurities.

Table 2. Laboratory measurement protocols for FIGIFIGO and SpectroClip-TR applied in the spectral measurements throughout this study.

FIGIFIGO	SpectroClip-TR
Spectrometer on (warm-up > 40 min)	Spectrometer on (warm-up > 40 min)
Lamp on (warm-up > 30 min)	Lamp on (warm-up > 30 min)
illumination zenith angle adjustment (**40**˚)	Optimization
Sensor zenith angle limits set (-40˚ to +40˚)	White reference for reflectance sphere
Sensor relative azimuth and zenith angles set (0˚)	Dark current
Optimization on white reference panel	White reference for empty reference sphere
Dark current	White reference for empty transmittance sphere
White reference meas.	Transmittance for adaxial leaf sample (#1)*
Target radiance meas.*	Reflectance for adaxial leaf sample
Sensor incremental turn in azimuth (15˚)*	Reflectance for abaxial leaf sample
⋮	Transmittance for abaxial leaf sample
Target radiance meas. (180° relative azimuth)	Transmittance for adaxial leaf sample (#2)*
White reference	Reflectance for adaxial leaf sample
Illumination zenith angle adjustment **(55**˚)	Reflectance for abaxial leaf sample
Sensor zenith angle limits set (-40˚ to +40˚)	Transmittance for abaxial leaf sample
Sensor relative azimuth and zenith angles set (0˚)	Transmittance for adaxial leaf sample (#3)*
Optimization on white reference panel	Reflectance for adaxial leaf sample
White reference meas.	Reflectance for abaxial leaf sample
Target radiance meas.*	Transmittance for abaxial leaf sample
Sensor incremental turn in azimuth (15˚)*	*One white reference for three consecutive leaf meas.
⋮	
Target radiance meas. (180° relative azimuth)	
White reference	
*Repeat up to 180˚ relative azimuth	

3.4 Data analysis methods

The main computing environment, used in both pre-processing of the data and in the analysis, was Matlab version 2017b. The BRF was calculated from the raw FIGIFIGO data using tools included in FGI Reflectance Toolbox. Similarly, SpectroClip-TR raw data was pre-processed in Matlab to reflectance and transmittance.

Individual spectra, obtained of both FIGIFIGO and SpectroClip-TR measurements, were smoothed using second order Savitzky-Golay filter with a 31nm window to improve analysis and interpretation. FIGIFIGO BRF single sample nadir spectra were as well averaged in analysis when applicable for improving the representativeness: nadir spectra of each relative azimuth orientation of the sensor (typically 13 spectra) were averaged into a single spectrum. The averaging of the FIGIFIGO BRF spectra were justified due to known fractioning of the total footprint between the individual field-of-views of the three spectrometer sensors [44]: visible near-infrared (VNIR, 350 to 1000 nm), short-wave infrared 1 (SWIR1, 1000 to 1800 nm), and short-wave infrared 2 (SWIR2, 1800 to 2500 nm) [54].

The analysis for the spectral anisotropy characteristics were done for both dwarf shrub species by evaluating the obtained BRFs as a function of three variables: wavelength,

view angle, and illumination angle. Although both spectrometers (ASD FieldSpec Pro FR with FIGIFIGO and ASD FieldSpec 4 Standard-Res with SpectroClip-TR) are capable of measuring radiance in 350 to 2500 nm spectral range, the spectral analysis in this study was limited to 400 nm to 2200 nm. This was done to exclude the noisy spectral ranges on both ends, a result of low value of irradiance upon the target surface at those wavelengths and thus a decreased signal-to-noise ratio, and to standardize the range between the methods.

The first part of the analysis concentrates on the spectral multiangular BRF observations on the principal plane. The measured BRF spectra of leaves-on samples are compared in 3D-feature space as such. Although spectral anisotropy can be approximated straight from the BRF surface plots, it is convenient to have a single number quantifying the anisotropy of the target surface. Averaged spectral anisotropy index ($ANIX_\lambda$) was applied to provide a single number for quantifying species anisotropy. ANIX is defined separately for each wavelength (or band) as the ratio of maximum and minimum reflectance factors obtained on the principal plane (or other azimuth plane) [55]. The formula for calculating ANIX is as in Equation 9:

$$\mathrm{ANIX}(\lambda) = \frac{R_{\mathrm{maximum}}(\lambda)}{R_{\mathrm{minimum}}(\lambda)}, \tag{9}$$

where $R_{\mathrm{maximum}}(\lambda)$ and $R_{\mathrm{minimum}}(\lambda)$ are the spectral maxima and minima reflectance factors obtained on the principal plane. ANIXs were calculated for each leaves-on samples of both species and further averaged to perform interspecies comparison of anisotropy.

View angle dependences of the BRFs were further analysed from four distinct view zenith angles on the principal plane. Three out of four angles (underlined) match those of MISR spaceborne instrument: +<u>26</u>°, <u>0</u>°, -<u>26</u>°, and -40°, where the positive angles indicate the sensor zenith angles into the direction of the illumination (backward), and the negative angles the sensor zenith angles away from the direction of the illumination (forward). Applying sensor zenith angles in the measurements that correspond to those of e.g. MISR was considered to extend the usage of data as ground reference in future applications.

View angle dependence and related anisotropy was as well analysed in multispectral dimensions, with chosen wavelengths matching those of Sentinel-2 satellite MSI instrument (Table 3). Due to large variations observed in the spectral BRF brightness, anisotropy factor (ANIF) was introduced to enable relative comparison of anisotropies in different wavelengths. ANIF is defined as the ratio of a given spectral BRF to the BRF in that same wavelength that is obtained from nadir view [55, 56], as shown in Equation 10:

$$\mathrm{ANIF}(\theta_i, \phi_i; \theta_r, \phi_r; \lambda) = \frac{\mathrm{BRF}(\theta_i, \phi_i; \theta_r, \phi_r; \lambda)}{\mathrm{BRF}_{\mathrm{nadir}}(\theta_i, \phi_i; \lambda)}, \tag{10}$$

where $\mathrm{BRF}_{\mathrm{nadir}}$ is the bidirectional reflectance factor obtained of the target from nadir view angle. Linear interpolation was applied to the BRF data of both species over the view angles between -40° and +32°. This was done to enable averaging of the measured sample spectra due to angular mismatch in zenith direction between goniometer measurements.

Table 3. Sentinel-2 MSI instrument bands and spatial resolutions

Sentinel-2(A) bands	Central wavelength (nm)	Bandwidth (nm)	Spatial resolution (m)
Band1 (coastal aerosols)	443.9	27	60
Band2 (blue)	496.6	98	10
Band3 (green)	560.0	45	10
Band4 (red)	664.5	38	10
Band5 (vegetation, red-edge)	703.9	19	20
Band6 (vegetation, red-edge)	740.2	18	20
Band7 (vegetation, red-edge)	782.5	28	20
Band8 (NIR)	835.1	145	10
Band8a (vegetation, red-edge)	864.8	33	20
Band9 (water vapour)	945.0	26	60
Band10 (cirrus clouds)	1373.5	75	60
Band11 (SWIR)	1613.7	143	20
Band12 (SWIR)	2202.4	242	20

Limiting the spectral BRF anisotropy analysis of heterogenous surfaces on the principal plane is supported by results of several previous studies [9,17,21]. These studies have shown the most radical changes in BRF occurring in the view angles approaching the illumination direction (backward direction) or the direction opposite to that (forward direction).

Due to importance and wide use of vegetation indices in earth observation, four indices were analysed for their dependencies on the chosen view angle, illumination angle, and for phenological changes induced by the growing season. The vegetation indices were Normalized Difference Vegetation Index (NDVI), Red-Edge Normalized Difference Vegetation Index (NDVI705), Moisture Stress Index (MSI), and Plant Senescence Reflectance Index (PSRI). The mathematical formulas for obtaining each index is shown in Table 4.

NDVI is well known and widely used index for normalizing reflectance factors obtained in NIR and red range wavelengths. These ranges represent parts of the spectrum where healthy vegetation induces high absorption and high reflection peaks due to chlorophyll absorption and leaves' internal scattering properties. Applications vary from land cover mapping to temporal estimation of leaf-area index. Although NDVI is a vegetation index, it can be used for mapping urban structures as well as water, snow and ice. The index range is normalized between -1 and +1, with typical dense green vegetation producing NDVI higher than 0.8. [57]

NDVI705 utilizes the wavelengths along the red-edge, and has thus higher sensitivity to changes in reflectance induced by green leaf pigments (chlorophyll) compared to NDVI. Red-edge is a term used to describe a spectral region in green vegetation reflectance spectrum, where chlorophyll in red (680 nm) and leaf's internal structure in NIR (730 nm) together result into a high spectral contrast commonly utilized in remote sensing of vegetation. Green leaf pigment content is connected to canopy properties such as canopy gap fraction and the level of senescence. The index range is the same as with NDVI. [58]

MSI is used to evaluate the stress conditions in the leaves induced by the changes in the water content. MSI is the ratio of reflectance obtained from a wavelength with high sensitivity to presence of water to reflectance obtained from wavelength with low

sensitivity to presence of water. As the water content increase the reflectance of the water absorption peak drops while the reflectance in NIR is nearly unaffected. Applications of MSI range from drought estimations to detecting vegetated areas that are under fire hazard. Temporal increase in MSI indicates smaller water content and typically elevated level of stress. MSI for vegetation and vegetated soils range from 0.5 to 1. [60]

PSRI is an index sensitive to the changes in chlorophyll and carotene pigments and is used in temporal studies of vegetation. In senescence the chlorophyll degradation induces an increase of reflectance in red while carotenes affecting mostly the blue band retain their absorption properties. PSRI has been also noticed to be sensitive to fruit ripening. [61]

Table 4. Spectral indices used in the analysis. The wavelengths applied were matched to the centre wavelengths of Sentinel-2 spectral bands.

Index	Formula (nm)	Sentinel-2 MSI bands	Reference
NDVI	$(NIR_{,835} - red_{,665}) / (NIR_{,835} + red_{,665})$	(Band8 - Band4) / (Band8 + Band4)	[57]
NDVI705	$(red\text{-}edge_{,740} - red\text{-}edge_{,704}) / (red\text{-}edge_{,740} + red\text{-}edge_{,704})$	(Band6 - Band5) / (Band6 + Band5)	[58]
MSI	$SWIR_{,1614} / NIR_{,835}$	Band11 / Band8	[59, 60]
PSRI	$(red_{,665} - blue_{,497}) / red\text{-}edge_{,704}$	(Band4 - Band2) / Band5	[61, 62]

The effect of the change in the illumination direction to the obtained nadir view reflectance factor from the shrubs was analysed by applying two distinct illumination angles (+40°, +55°). Both angles represent growing season solar zeniths at the given latitudes of the study areas. The spectra in this analysis represent the average of nine leaves-on samples of both species, each being an average of 13 azimuthal nadir measurements. Illumination direction analysis was applied to the same four vegetation indices introduced previously, with a hypothesis of some of the indices being more affected by the variation in the illumination zenith angle than others. This information is useful in multitemporal studies of vegetation where the solar zenith may not be the same between the acquisition times.

The effects of seasonality and the related spectral changes in the measured radiance were studied through vegetation index analysis. The four indices selected in the analysis were the same introduced earlier. The seasonality of the dwarf shrubs was studied to see if a particular phenological stage enable more reliable species identification, and if some of the indices act as better indicators of leaf growing, flowering, berrying and senescence than others. Each presented index data point is calculated from an average spectrum of 13 nadir BRF measurements, obtained under illumination zenith angle of +40°. The samples were measured as they were found in the nature and thus presented one of the four phenological stages. The measured samples are shown in Table 5.

Table 5. Phenological stages of the BRF shrub samples measured and analysed for temporal spectral changes.

Blueberry	Stage	**Lingonberry**	Stage
B_spring	Leaves-on		
B1	Leaves-on	L1	Flowering
B2	Leaves-on	L2	Leaves-on
B3	Leaves-on	L3	Flowering
B4	Flowering	L4	Flowering
B5	Leaves-on	L5	Leaves-on
B6	Berrying	L6	Berrying
B7	Berrying	L7	Berrying
B8	Berrying	L8	Berrying
B9	Berrying	L9	Berrying
B_autumn	Leaves-on		

The final spectral analysis concentrated on providing information on the contribution of berries and flowers on the overall spectra. The analysis was done from sensor nadir view angle, from where berries and flowers were expected to be most visible due to maximum canopy gaps. The nadir view was further justified with a previous study on the forest reflectance where the contribution of the understory was evaluated in multiangular measurement geometry, and where it was shown that the largest contribution is observed from close-nadir view [16].

4 Results and discussion

Changing the view angle of the observer relative to the target can have either a large, small, or no effect on how the target appears to the observer. The induced differences in the appearance depend on the optical properties and the 3D-structure of a target, the spectral irradiance, the relative illumination direction and geometry, and the view direction. The radiance from the target surface into the direction of the observer is a function of both the view and illumination angles, and of the wavelength. This change in radiance was expected to be relevant to this study since both lingonberry and blueberry have been previously noted to have a specular component into the forward scattering direction, and a strong hotspot component into the direction of the illumination [17].

4.1 View angle dependence

4.1.1 Overview

An overview photo series is shown in Figure 18, illustrating the change in the visual appearance of a dwarf shrub sample as the view angle is tilted. The photos illustrate how the sensor tilting into the direction of the illumination induces brightening of the sample. This is due to decrease in gap fraction, and increase of shadow-hiding and coherent backscatter effects [19]. At the hotspot measurement geometry at +40°, the self-shadowing of the sensor prevents collecting meaningful data from the target. Tilting away from the nadir view into the forward direction introduces a darkening backshadow effect at gentle forward zenith angles between 0° to -20°. At these angles the sensor sees parts of the canopy that are shadowed by the foliage itself [55]. Tilting the sensor to its extreme forward angle (-40°) introduces a strengthening of the specular component, brightening the leaves to appear nearly white in colour [55].

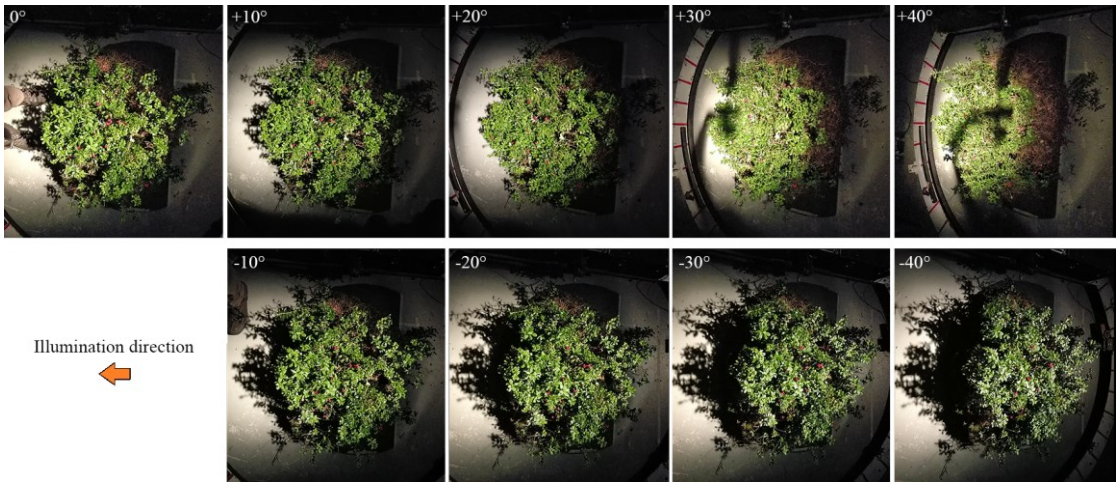

Figure 18. A multidirectional photo series illustrating change in the appearance of a lingonberry shrub sample as the view angle zenith is changed. The illumination is at +40°, from the right-hand side of the photos to the left. The photographs were taken with a smartphone camera which was held manually next to the FIGIFIGO sensor optics at the given angles. Photographer's feet, and the shadow of the hand holding the camera appear in the photos.

Spectral contour plots in Figure 19 show visualizations of the spectral data included in the view angle dependence analysis. The analysed data were obtained from leaves-on shrub samples on the principal plane between DOY 152 and DOY 256.

Samples of both species show brightening into the illumination direction and a discreet brightening into the forward direction (Figure 19). This is most noticeable in the contour plots in green (560 nm), NIR (700 nm to 1400 nm), and SWIR (1700 nm). The reflectance factor peak is obtained from both species in 1070 nm into near-backscattering direction. The bright peak averages to 0.65 units for lingonberry, and 0.54 units for blueberry. In the average lingonberry produces a 20% brighter BRF peak compared to blueberry in both backward and forward scattering directions.

The observed sharp contrast between the red (660 nm) wavelength and the beginning of NIR (750 nm) region is typical for healthy green vegetation (Figure 19). The spectral contrast is caused by the absorption properties of chlorophyll within the leaves, and the leaves' internal reflection properties. Chlorophyll pigments absorb strongly in VIS, especially in red, while in NIR the high reflectivity is caused by the internal scattering of longer wavelength radiation from leaves' cell walls [63]. In a canopy structure, the spectral contrast between the BRFs obtained in VIS and NIR are further amplified by the induced shadows and the natural multiple scattering environment within the canopy, and between the foliage and the soil. These introduce spectral changes in the optical interactions which are observed in measured spectra. Radiation in the VIS range is strongly affected by the multiple scattering environment which increases the probability of energy absorption. On the other hand, the absorption in NIR is low, and thus rather than being absorbed, the radiation is scattered diffusely within and away from the canopy. [64]

In Figure 19, the red edge in 700 nm, and the two water absorption peaks in 1400 nm and 1850 nm can be identified by taking a note of the visual densification of the drawn contour lines. The contour line densification indicates a rapid change in reflectance factor. Samples such as lingonberry L3, L4, L9, and blueberry B1, B8, and B9, show an increase in NIR reflectance from nadir view, indicating an increase in gap fraction and thus an increased contribution from illuminated underlying soil [16]. On the other hand, samples such as lingonberry L2, and blueberry B2 and B7, show a decrease in reflectance factor from nadir view indicating presence of deepening shadows. When comparing the BRF contour plots in photographs taken from each sample from nadir (see Appendix A), the presence of shadows and illuminated soil in the sensor footprint supports the observations made of the reflectance factors.

Differences in the 3D structures and leaf orientations can be identified in the BRF data as the sources of between-species and between-sample variations, both into the backward and forward scattering directions. An example of a structural dependence is shown in Figure 19 with blueberry sample B6, where an extended backshadowing results the sensor to measure radiance from a shadowed shrub in all forward viewing directions on the principal plane. The result is a spectrally relatively flat BRF surface. BRF obtained from blueberry sample B2 on the other hand shows a strong forward scattering component, indicating a more evenly distributed canopy cover.

Similar observations on the spectral variations on the heterogenous surface BRFs of lingonberry and blueberry have been previously reported [17]. When measuring a heterogenous volume, even a small change in the measurement location has been shown to have a large impact on the measured radiance [17]. The spectral heterogeneity from a given view angle is a sum of contributions from all the scattering elements included in the shrub sample. The biophysical properties and orientations of the leaves, 3D structure

of the shrub, canopy gap fraction, the underlying soil and vegetation, leaf and soil moisture, and the illumination angle all contribute to the overall radiance. The spectral variability between tree leaves of a same species sharing the same phenological stage have been shown to be relatively small [50, 65, 66]. Thus, for shrub samples measured during the summer months, the within-canopy optical dynamics are speculated to be less effected by the variations in the optical properties of individual leaves, and more by their orientation, distribution and the general shrub structure.

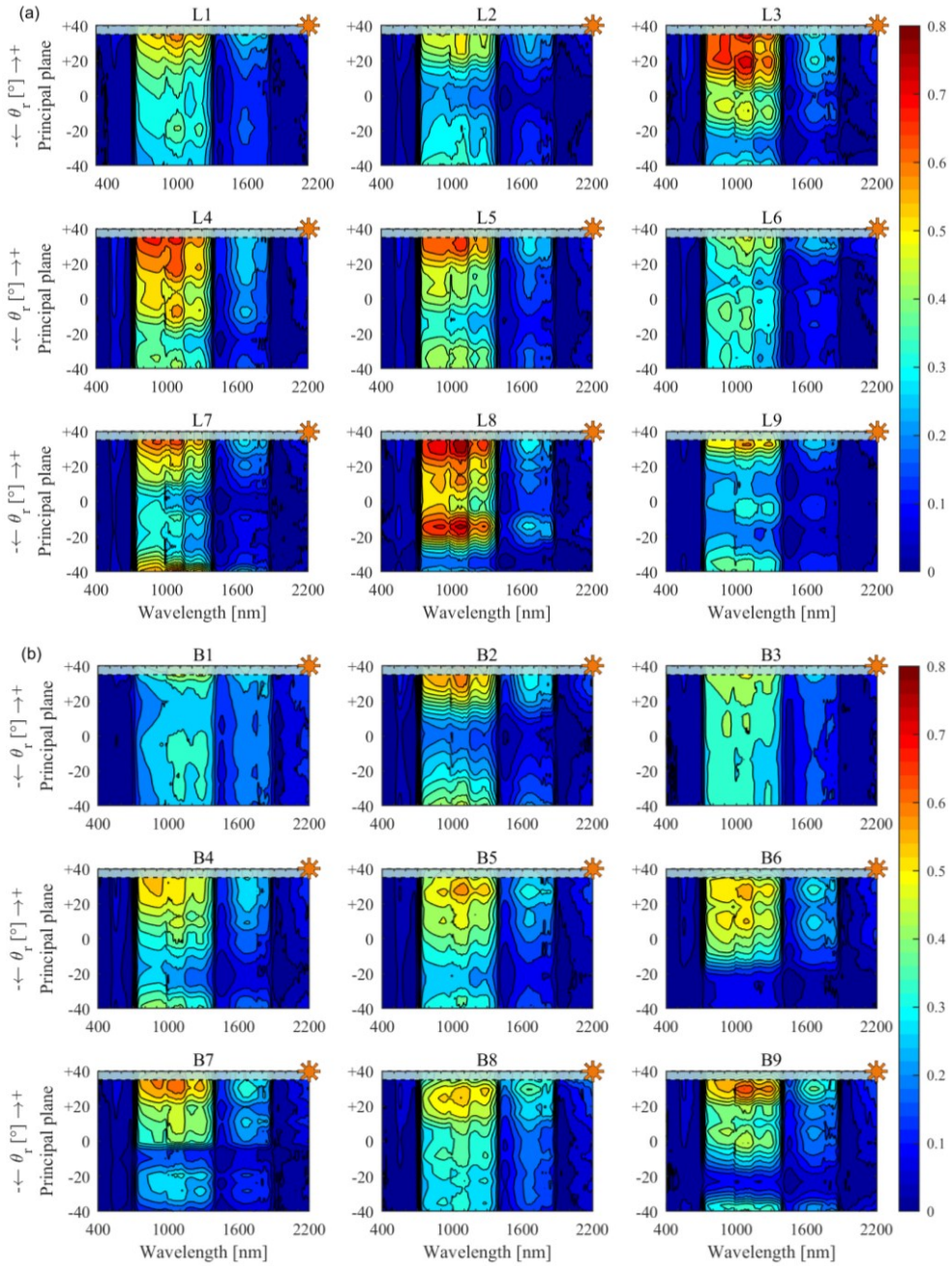

Figure 19. Spectral contour plots of reflectance factors obtained on the principal plane of (a) lingonberry samples L1 to L9 and (b) blueberry samples B1 to B9. All samples represent the leaves-on phenological stage. The illumination zenith angle is noted with a sun-symbol at +40°, where also a blue zone of 5° is drawn to block interpretation of the data in the sensor self-shading region.

4.1.2 Anisotropy index

To numerically compare the spectral anisotropies of blueberry and lingonberry as species, an averaged spectral anisotropy indices ($ANIX_\lambda$) were calculated. As given in the description of ANIX in Chapter 3.4, the index is the spectral ratio of the maximum and minimum reflectance factors obtained on the principal plane (Figure 20). Spectral ANIX provides an intuitive single spectral quantity of the species anisotropies, and thus enables comparative analysis [55].

The averaged anisotropy indices of the dwarf shrub soils shown in Figure 20.a share a similar spectral curvature, and are closely matched throughout the spectrum. The soil indices stay mostly between ANIX 1.6 and 2, with low spectral variability and small difference between the maximum and minimum. These spectral characteristics have been noted earlier to indicate isotropic scattering from non-vegetated surfaces [55, 56]. However, the soils in this study measured a great majority of the spectral BRF maxima into the backward scattering direction at sensor zenith angle +32° to +38°, while the minima were scattered with a large angular distribution between -5° and -40° (not shown). This indicates a low spectral sensitivity to changes in the view angle, but also BRF view angle anisotropy towards the illumination source. The shown soil ANIX profiles deviate from ANIX of a concrete slab which was presented in the given literature reference [55]. This is because soils in general consists of spectrally rough elements with complex scattering properties, has spatially varying moisture content, and because small amount of moss and grass was noted growing on the samples [8]. The soil roughness has an impact through introducing shadowed areas and by increasing multiple scattering compared to solid flat surfaces [8]. The small amount of vegetation was speculated to have contributed on the measured radiance, with a result of the spectral soil ANIXs to follow the profiles of the shrub ANIXs, only at lower index.

Compared to the indices of the soils, the averaged dwarf shrub ANIXs (Figure 20.a) are larger throughout the spectrum, as are their spectral variations. The change in index is especially prominent when moving in the spectral domain from VIS into NIR wavelengths. When considering spectrally the maximum and minimum BRFs, the difference is relatively large. This can be taken as an indicator of an anisotropy where the incident radiation is scattered by the surface mostly in some distinct directions [55]. Spectral interspecies comparison of the leaves-on samples show that blueberry produced 41% larger index in VIS, with ANIX larger than 4 in blue wavelengths. The index profiles obtained from blueberry and lingonberry are in line with those reported earlier on watercress [55], and on lingonberry and blueberry [17], although displaying somewhat larger index. The differences of the calculated ANIX to those of the watercress measurements [55] are speculated to be caused by the interspecies differences in biophysics and related optical properties in the leaf and canopy levels, as well as different illumination setup. The difference to the ANIXs of earlier measurements made on the same dwarf shrub species [17] are likely a result of natural variations in the optical properties, occurring within relatively small sample population when measuring heterogenous surfaces.

Both species produced higher ANIXs in VIS than in NIR. In visible region the chlorophyll and carotene pigments absorb electromagnetic radiation strongly in blue, green, and especially in red. In Figure 20.a, both blueberry leaves-on shrub samples and blueberry soil samples display a peak in the index in red wavelengths around 680 nm, and a small dip in green around 560 nm. These indicate an increase of spectral anisotropy when chlorophyll pigment is strongly present in the sample. On the other hand, in NIR

where the effect of chlorophyll is minimal in green vegetation, and leaves' internal structure causes high reflectivity, ANIX is low. [55]

Elevated ANIXs in 1450 nm and 1940 nm are located at the water absorption regions, where the uncertainty in the spectral ratio of maxima to minima increases as seen in the 95% confidence interval plots in Figure 20.b. The 95% confidence intervals show the expected range of future sample ANIX around the mean value. Both soils show spectrally levelled uncertainties compared to the shrub samples with only small deviations from the mean values. When comparing the expected ANIX of blueberry shrubs to that of lingonberry shrubs, blueberry shows considerably higher uncertainty up to 1500 nm. This is an indicator that there exists a larger between-samples spectral anisotropy variation in the measured blueberry population than between the two dwarf shrub species. The large spectral between-samples variation of blueberry is speculated to be because of a combination result of varying leaf orientations in a complex 3D shrub structure, variations of the shadowed areas increasing the spectral heterogenous response, larger transmittance of the leaves, and variations in the gap fraction. By visually comparing the adaxial and abaxial sides of the leaves of the two species, the thin blueberry leaves seem to transmit more light through the leaves into the canopy structure. This is speculated to induce a strong contribution of the underlying vegetation and soil in the resulting BRF spectra, and thus increase the between samples anisotropy.

The two noticeable jumps in the ANIX profiles in Figure 20 displayed in 1000 nm, and in smaller extent in 1800 nm, are caused by a combination error involving the three sensors of the spectrometer, the spatial heterogenous nature of the target surface, and the unevenness of the instrument optics' field-of-view [13, 44].

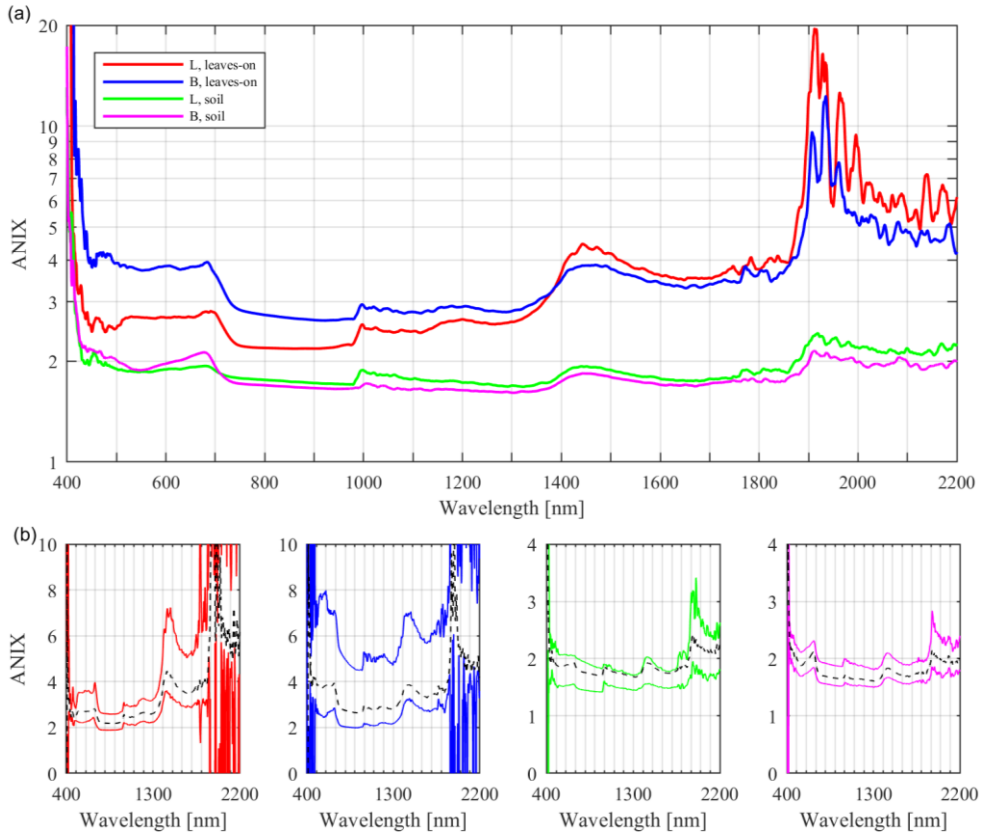

Figure 20. (a) Averaged spectral ANIX of leaves-on shrub samples and (b) the associated 95% confidence intervals.

Distributions of the view angle dependent spectral minima and maxima reflectance factors on the principal plane are shown in Figure 21. These were previously used in the calculations of the averaged ANIXs. Both species are shown to produce angularly largest spectral BRF contrast near the edges of the spectrum, namely between 400 nm and 500 nm, and 1800 nm and 2200 nm. Lingonberry in Figure 21.a has an angularly narrow distribution of maxima at sensor zenith angles larger than +30° into the backward direction, while blueberry maxima are obtained from a wider, and thus more forward biased range of sensor zenith angles larger than +24°. Although both species have angularly widely scattered minima, blueberry shows densification of points between sensor zenith angles -45° and -40°, and around -20° with only a few points into forward viewing direction.

The associated bar graphs in Figure 21.b show the angular distribution of maxima and minima BRFs in percentages. Lingonberry has widely spread minima at sensor zenith angles less than +10°, with an elevated nadir region containing 18%, and a forward region between -30° and -20° containing 27% of the minimum points. Blueberry is shown to have 8% of minima distribution around nadir and two forward peaks around sensor zenith angles +22.5° and -40°, containing 24% and 26% of minima BRFs respectively. More than 80% of the maxima spectral reflectance factors are obtained for both species at sensor zenith angle larger than +25°, with a distribution peak for lingonberry of 47% maxima between sensor zenith angles +30° and +35°.

A densification of angular BRF minima was observed between sensor zenith angles -5° and -30° for both species. The backshadowing effect, a result of foliage shadowing itself [55] results approximately 50% of the minima to be found at these viewing angles. The maxima BRF distribution is concentrated around the near-hotspot geometry. This was an expected result for a canopy type of structure [20], where the amount of shadowed target surface is minimal at hotspot due to shadow-hiding phenomenon [19].

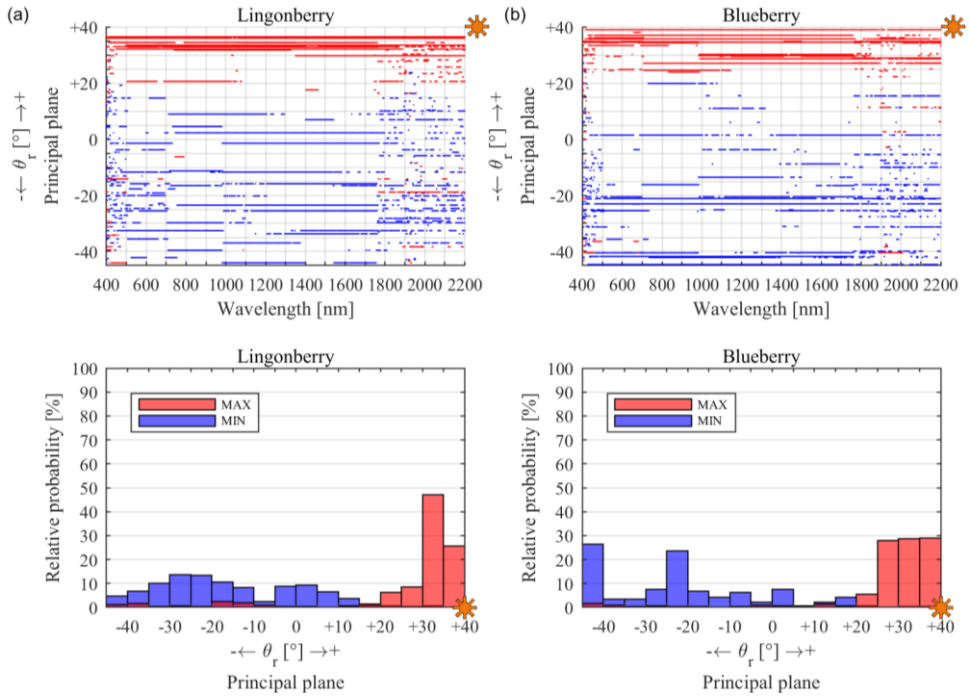

Figure 21. Angular distributions of minimum and maximum BRFs obtained on the principal plane of (a) lingonberry and (b) blueberry.

4.1.3 View angles

The averaged BRF spectra of lingonberry and blueberry show strong anisotropy into the backward viewing direction (Figure 22) of both leaves-on and soil samples. Both soils produce a BRF ratio of 125% in NIR, when comparing the BRFs obtained from the sensor zenith angle of +26° to that obtained from the nadir view. The soils show interspecies similarity in the BRF view angle dependency and are spectrally similar. Following this observation, any observed spectral interspecies differences resulting from shrub sample comparison analysis are considered to be caused by the properties of the shrubs themselves.

When comparing the BRFs of the leaves-on samples of the two species, lingonberry is brighter in VIS and through NIR, but weaker in SWIR after 1350 nm (Figure 22). The larger BRF of lingonberry in the visible wavelengths is prominent in forward viewing directions into sensor zenith angles +26° and +40°, where the ratio to blueberry is more than 170%. A dip in the lingonberry to blueberry leaves-on ratio is noticed around the chlorophyll absorption peak in red wavelengths. The interspecies difference in the forward biased anisotropies indicate a difference in the optical properties of the two dwarf shrubs, favouring the leaves and shrub structure of lingonberry over blueberry for specular reflection component [67]. Leaf biophysical and physical properties, such as leaf thickness and internal structure, glossiness of the adaxial side surface, water and pigment content all affect the spectral anisotropy [67, 68]. Since the measured lingonberry and blueberry shrub samples are volume scatterers, the species with more horizontally distributed glossy leaves is expected have a stronger specular component. The strength of the specular component is further increased by the minimum gap fraction in extreme forward direction [16].

Both species show strong directional radiance into sensor zenith of +26°, with lingonberry producing a backward to nadir BRF ratio exceeding 200% in SWIR (Figure 22). The large backward scattering ratio of lingonberry is speculated to be caused by the characteristic shadow-hiding properties, further strengthening the contribution of the internal scattering of longer wavelengths within the leaves.

In wavelengths longer than 1350 nm however, blueberry is observed as brighter in all evaluated view directions (Figure 22). The decrease of lingonberry BRF in the longer wavelengths indicates an increasing effect of the sample water content. The lingonberry leaves were expected to have a higher relative water content due to thicker leaves compared to blueberry. In SWIR the water absorption seems to dominate over the strong backward scattering properties of lingonberry which produced high reflectance in all view directions in VIS and NIR.

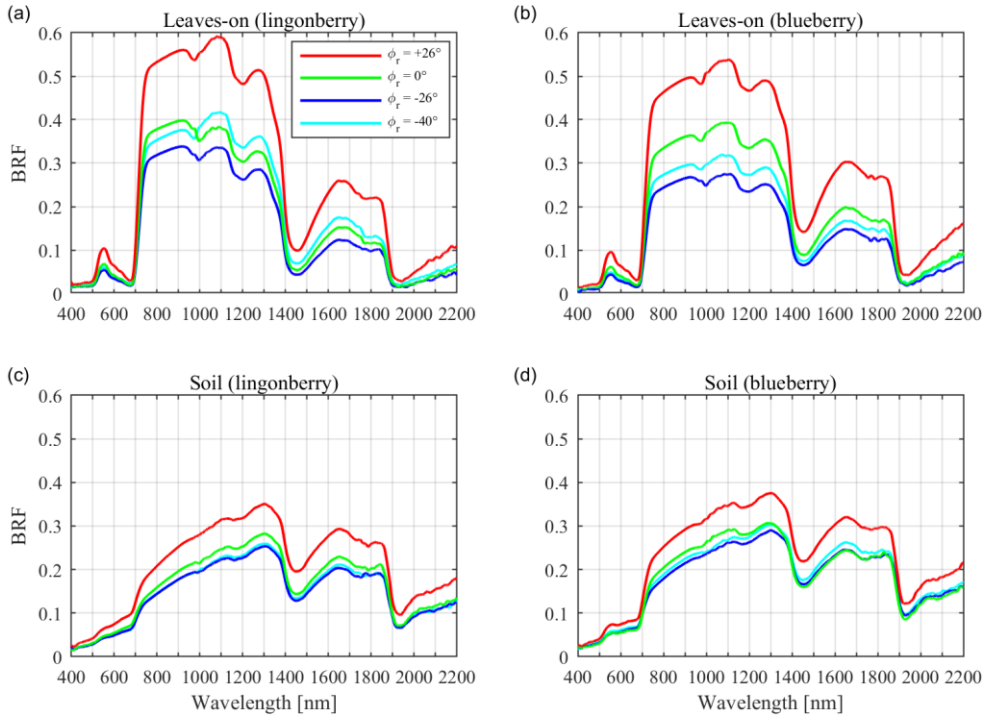

Figure 22. Averaged spectral view angle dependence of (a) lingonberry and (b) blueberry leaves-on shrubs, and (c) lingonberry and (d) blueberry soils. View zenith angle +26°, 0°, -26° match the fixed camera angles of MISR satellite instrument while -40° represents the extreme forward direction directly opposite to illumination zenith angle +40°.

4.1.4 Multispectral

To relate the observed reflectance factor's view angle dependencies to an existing earth observation application, a specific selection of spectral shrub sample BRFs were plotted as a function of view angle (Figure 23). The shown anisotropy factors (ANIF) follow the definition given in Chapter 3.4.

In Figure 23.a, the change in view angle is shown to have a strong anisotropic brightening effect on measured spectral BRF. In the low absorptance wavelengths in NIR (740 nm and 835 nm), lingonberry BRFs show a change of 0.2 units when the sensor is tilted from nadir into backward direction of +32°. Similarly, blueberry displays 0.15 units increase in BRF towards the illumination source. Both species exhibit spectrally lowest BRF into gentle forward direction at sensor zenith angle of -28°, but show as well characteristic forward scattering into far forward sensor zenith angles smaller than -28°. Both species display strong anisotropies in the two SWIR wavelengths (1614 and 2202 nm) with ratios of near-hotspot maximum to minimum ANIF larger than 235%. This was earlier speculated to be a result of an increase in within-leaf scattering into direction of illumination, with an amplifying contribution from the thicker leaves of lingonberry (Figure 22). Although the BRF in wavelengths 740 and 835 nm show significant increase in BRF, the actual anisotropy at NIR band is one of the smallest. This is because NIR reflectance has a high tolerance to varying shadows in the canopy. Shadowed parts of the canopy introduce a multiple scattering environment that increases the probability of chlorophyll absorbing the energy contained in the VIS wavelengths [55].

In Figure 23.b, the relative strongest scattering into the forward viewing direction occurs in blue (497 nm), red (665 nm), and in the two SWIR bands 1614 and 2202 nm. This is similar with both species. Chlorophyll content in the leaves seems to suggest a spectral dependence of the anisotropy into both zenith directions on the principal plane [55].

The plotted BRFs represent spectral averages of angularly interpolated data points. The spectral responses were restrained to maximum sensor zenith angle of +32° into the illumination direction. This was done because of the existing constrains related to the angular resolution of the measured data, and to prevent interpretation close to sensor self-shadowing region at sensor zenith angle +40°.

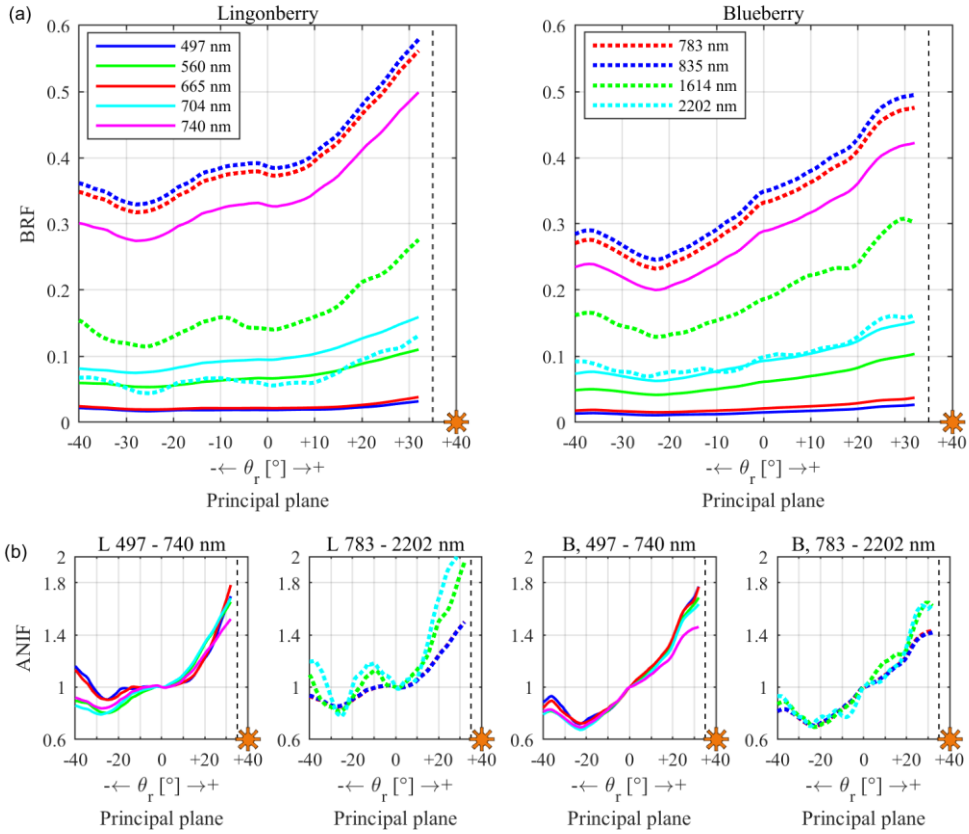

Figure 23. Averaged leaves-on sample multispectral (a) reflectance factors and (b) anisotropy factors on the principal plane as a function of sensor zenith angle. The wavelengths match Sentinel-2 MSI instrument centre wavelengths on bands 2 to 12.

4.1.5 Vegetation indices

View angle dependencies of four vegetation indices are presented in Figure 24. The selected vegetation indices were NDVI, NDVI705, MSI, and PSRI, and were given definition in Chapter 3.2. The four indices can be applied for evaluation of greenness of vegetation (NDVI, NDVI705) [57, 58], water content and related stress (MSI) [59], and senescence and berry detection (PSRI) [61].

When illuminating the samples from +40° zenith angle and evaluating the effect between sensor zenith angles -40° and +32°, a 3% variation in NDVI was observed (Figure 24). The highest NDVI, 0.90 was reached for lingonberry at sensor zenith angle

+15°. High NDVI indicates high spectral contrast between NIR (835 nm) and red (665 nm), and is commonly related to healthy green vegetation [63]. With blueberry, the highest NDVI of 0.89 was determined from nadir view BRFs. The general profiles of the calculated NDVIs are similar between sensor zenith angles -35° and +32° with both species. A pronounced decline of the index is shown with both species towards the extreme sensor zenith angles. The presented multidirectional NDVIs are in line with previous studies on vegetated targets involving hyperspectral goniometer measurements [21] and satellite data [69]. Interspecies comparison shows a maximum of 2.6% difference in index into gentle backward view zenith angle of +21°. Beyond the sensor zenith angle of -35° in extreme forward direction, blueberry displays a further increase in index of 1%. According to the obtained results, the NDVIs are similarly dependent on the view angle with both species.

The shown NDVI705 view angle dependence is more linear than that of NDVI, with a decline into the illumination direction (Figure 24). Both species show higher NDVI705 into extreme forward view direction, 0.58 and 0.52 for lingonberry and blueberry respectively, and lower index towards the illumination source, 0.52 and 0.47. The forward to backward ratios are very similar between to two dwarf shrub species: 110% for lingonberry and 111% for blueberry. Interspecies comparison shows that lingonberry produces up to 12% higher NDVI705 in forward and backward directions, but less than 7% higher near nadir. Since NDVI705 utilizes BRF in 704 nm wavelength, rather than the 665 nm used to calculate NDVI, the index is less responsive to the backshadowing effect which in NDVI induced a strong change due to increased red absorption. This results NDVI705 to have lower sensitivity to changes in the view zenith angle.

When comparing the angular BRFs of individual wavelengths (Figure 23), the measured BRFs from both species are similar in 704 nm, while in 740 nm blueberry produces lower BRF over the analysed angular range. The explanation for the interspecies differences in NDVI705 arises from the differences in the leaf spectra at these two wavelengths, of which 705 nm is spectrally located at beginning of the red-edge and 740 nm at the end of the red-edge. As will be later shown in the results of this study (Chapter 4.3), the leaves of lingonberry are spectrally notably brighter in 740 nm wavelength (up to 30%) compared to blueberry leaves while inseparable in 704 nm.

Both lingonberry and blueberry produce MSIs with profound bowl like curvature describing the view angle dependence within the given angular range (Figure 24). Moisture stress index detects changes of water content in plants by calculating the ratio of the reflectance factor obtained in SWIR (1614 nm) to that obtained in NIR (835 nm). Since SWIR range has high sensitivity tolerance and NIR range low sensitivity to the effects of increased moisture content, the increase in the ratio indicates decrease of water content, and vice versa [60]. When compared to the indices obtained from nadir, the indices into forward view direction show 17% and 7% brighter for lingonberry and blueberry respectively. In backward direction the ratios are 31% and 10%. Based on the obtained results, lingonberry MSI is more strongly affected by the sensor zenith angle than blueberry in the given angular range. Interspecies comparison shows blueberry producing up to 155% MSI into the sensor zenith angle of -30°. Similar ratio was observed into the gentle backward directions between nadir and +15°. In sensor zenith angles around -10° and -20° the ratio is around 130%, where the decrease in index ratio is speculated to be caused by the interspecies differences in the optical characteristic of the leaves: the wax residing on top of the adaxial side of lingonberry leaves was expected induce specular reflection through altering the optical index and surface roughness [70]. As the sensor zenith tilts further forward, a strong backshadowing effect increases the

effect of water absorption in SWIR, thus decreasing the MSI. Based on the similarities in spectral responses of the soils, the calculated MSI indicate that lingonberry leaves have a larger relative water content compared to blueberry leaves.

The fourth index included in the view angle dependency analysis was PSRI (Figure 24). PSRI is a vegetation index used to detect mainly senescence but also berry ripening of green vegetation [61]. The detection is based on evaluating the spectral effects of chlorophyll degradation as the season progressed. The calculated PSRIs display angular tolerance with maximum change of 0.01 units between sensor zenith angles -40° and +28°. Approaching the illumination zenith angle, both species show an increase in the indices, indicating a higher responsiveness into hotspot measurement geometry. Interspecies comparison shows blueberry having a higher PSRI of 0.04, which is more than 200%. This results from a larger difference of BRFs obtained in red and blue wavelengths, and lower BRF in the red-edge (Figure 23). It can be speculated, that the red-edge located in 705 nm is darker with blueberry over the given angular range due to higher transmittance of blueberry leaves. This would lessen the strength of the specular component. Also, the spectral radiances measured from blueberry are lower in red, and especially in blue compared to lingonberry (Figure 23). The larger difference in BRF between red and blue increases PSRI.

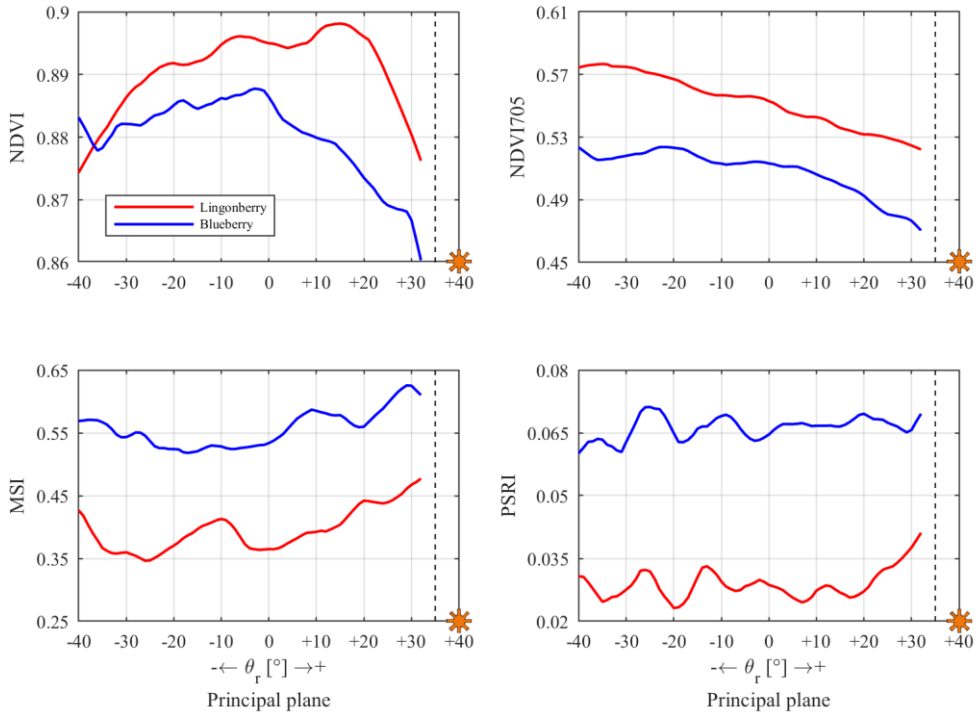

Figure 24. View zenith angle dependence of four vegetation indices. The illumination zenith angle is noted with the sun-symbol at +40°.

4.2 Illumination angle dependence

Spectral measurements of reflectance anisotropy as a function of illumination direction provide useful information for the analysis of field data. Spectral BRF of lingonberry in Figure 25.a, shows a very limited response to the change in the illumination zenith angle while the response of blueberry is noticeably stronger. Lingonberry can be thus considered spectrally more tolerant in this aspect of the two species. Blueberry displays a response with an increase of reflectance factor up to 0.07 units in NIR, as the illumination zenith increases 15°. In Figure 25.b, the calculated BRF ratios of the two illumination zenith angles show steady spectral responses: 15% increase for blueberry between wavelengths 450 nm and 1900 nm, and a 2% variation for lingonberry. In VIS range, lingonberry has a small peak in the ratio around 680 nm, not visible with the ratio of blueberry. The brightening of lingonberry in red is speculated to be caused by an increase in red band absorption at smaller illumination zenith angles. This is due to shadowed parts of the canopy which have a larger spatial coverage at smaller illumination zenith angles [55].

Species separability is shown to be improved at the steeper illumination zenith angle of +55˚, where in NIR the interspecies difference in BRF is more than 13%. At +40° the spectral reflectance factors of lingonberry and blueberry leaves-on shrubs are close to identical. The drawn confidence intervals show that with lingonberry the change in the illumination zenith angle is not spectrally separable due to consistent overlapping of intervals. With blueberry, the separation is clearer with some 10% overlap of the intervals, increasing the reliability of the observation of the characteristic dependency of blueberry.

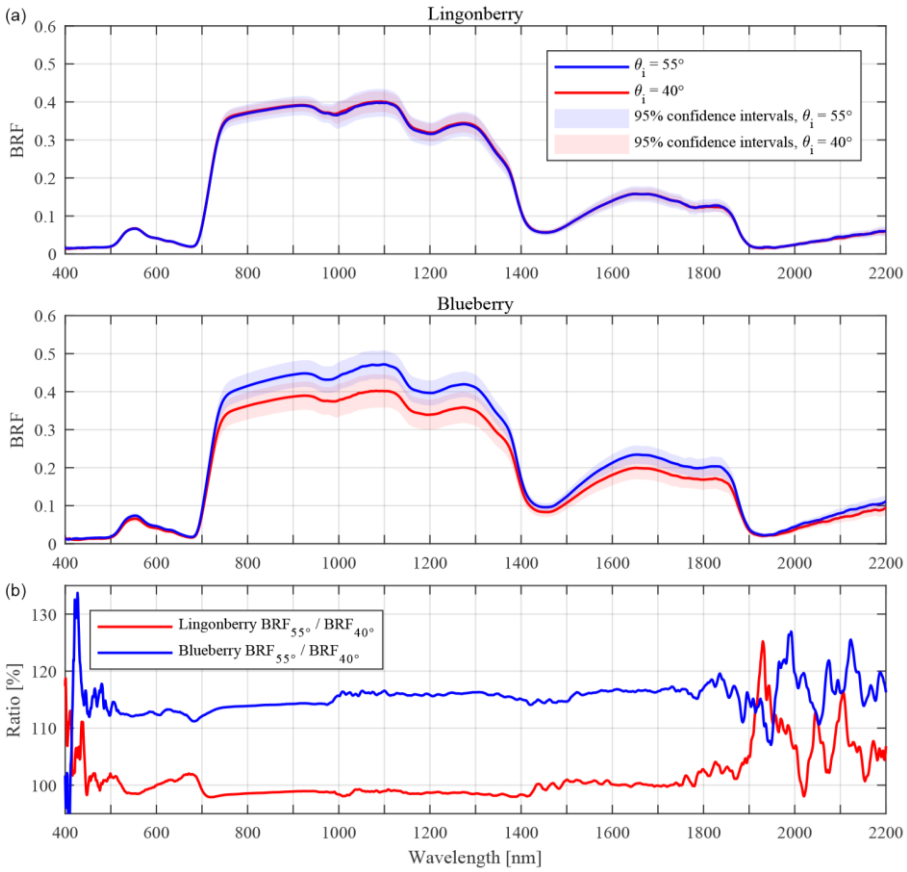

Figure 25. Spectral reflectance factor dependencies on two illumination zenith angles of (a) lingonberry and blueberry, with (b) calculated ratios.

Analysis of the spectral effects of changing illumination direction was extended to four vegetation indices. (Figure 26). The maximum change of 5.4% is observed with lingonberry PSRI, 0.00158 units, while rest of the indices show a change between 0.3% and 2.7%. The smallest changes were observed with the two NDVI indices which both produced ratios less than 1%. In interspecies comparison, three of the four indices show opposite trend directions as the illumination zenith angle is increased by 15°, MSI being the only exception with a shared positive trend.

As the illumination zenith angle increases, less of the soil and more of the canopy top is illuminated. This decreases the contribution of soil to the overall radiance leaving the canopy towards the sensor. The contribution of the soil has relevance as its spectral response to incident radiation is different from green vegetation (Figure 22). Larger leaf area over the soil induces a decrease in the obtained reflectance factor in red wavelengths due to increased absorption.

The four indices in Figure 26 show low sensitivity to the changing illumination zenith angle. This is because the indices represent the spectral contrasts and not the BRFs as such. Thus, even though the BRF of blueberry was shown to be affected 15% by the 15° change in illumination zenith angle (Figure 25), the change in the indices is relatively small. For example, NDVI of blueberry is affected only by 0.3%.

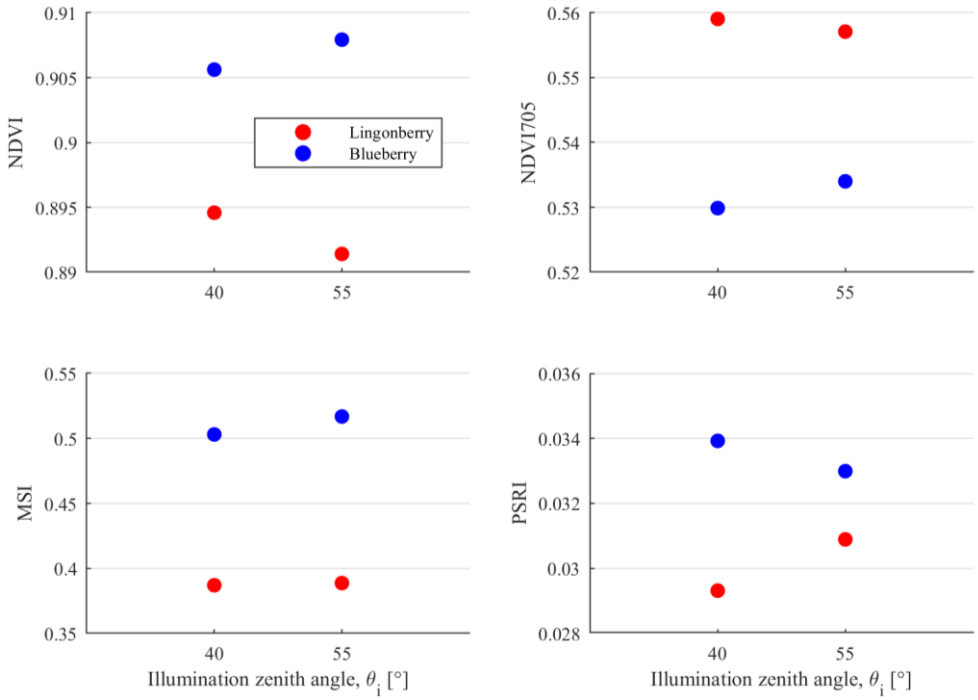

Figure 26. Four vegetation indices calculated from nadir view BRF as a function of two distinct illumination angles.

4.3 Temporal dependence

The temporal analysis was based on the lingonberry and blueberry shrubs in their natural phenological stages, and on leaf spectra, analysed for seasonal spectral variations (Figure 27). The seasonal variations were observed from effects on four different vegetation indices, calculated from nadir view spectra. These four indices were defined earlier in Chapter 3.4.

Blueberry NDVI in Figure 27 changes 0.24 units between the spring sample (DOY 144) and the mid-summer sample (DOY 188), from 0.69 to 0.93 respectively. This change in NDVI indicates a seasonal variation where the shrub greenness is densified through growing of leaves and emerging of underlying deciduous soil vegetation. Similar change is not evident with lingonberry due to evergreen nature of the species, although it should be noted that the first lingonberry sample was not measured until DOY 158. During the measurements made in the summer (DOY 153 up to DOY 247) blueberry NDVI ranges from 0.87 to more than 0.93, while lingonberry produces NDVI between 0.83 and 0.92. Comparing the NDVIs of the summer samples to the autumn samples, measured between DOY 251 to DOY 272, the seasonal changes are evident in both the BRF and the SpectroClip-TR data as a decrease of index. Observations from SpectroClip-TR leaf reflectance data follows the temporal characteristics of the BRF data from late summer to autumn, although differing in magnitude. This magnitude difference between shrub and leaf NDVIs is related to the spectral contrasts residing in the data collected at different spatial scales of the target. Differences of the spectral contrasts have been previously studied [71] and it has been shown that the radiance from red and NIR bands is higher from individual leaf surfaces than from canopy structure, with the red band reflectance factor being the relatively higher of the two. This is due to the lack of the 3D structure of the canopy and related shadows when measuring individual leaves. The smaller spectral contrast between BRF in red and NIR of the leaves results a lower NDVI.

The NDVI of the blueberry shrubs changes more than 10% of the entire index range of 2 units from spring to summer (Figure 27). As the leaves develop, the underlying soil gets covered and the leaves contribute more strongly on the measured radiance. This induces an increase in NDVI due to increased spectral contrast between reflectances from red and NIR wavelengths. An inverse phenological phenomena is visible in the autumn NDVI of blueberry (DOY 274) with an induced drop in the index of 0.13 units. In the autumn, the leaves of deciduous plants start to lose their chlorophyll content, resulting a change in the optical properties of the leaves. The red-edge loses some of its spectral contrast due to degradation of chlorophyll content which increases the red reflectance, while leaves' internal cell wall structures are broken down which decreases the NIR reflectance.

With lingonberry, the variation in NDVI is shown to be less than 0.08 units during the summer months (Figure 27). Lingonberry samples measured on DOY 158, DOY 173, and on DOY 178 included flowers. The flowers are speculated to have influenced the NDVI by increasing the red band reflectance, and thus decreasing the spectral contrast between red and NIR. Lingonberry flower petals contain non-photosynthetic pigments and are mostly white with a red tint in appearance (Chapter 1.3, Figure 12). The white colour of the lingonberry flowers induces a brightening of the three flower bearing shrub samples in red wavelengths, with relatively small brightening in NIR, resulting a reduction in the calculated NDVI. Following the same reasoning, the presence of considerable number of red coloured berries induces a similar reduction of NDVI. Lingonberry shrub samples with berries were measured on DOY 251 and 256. The presented temporal NDVI profiles

agree with those from previous spectral studies on seasonal dynamics of understory vegetation [72], with a spectral fit to temporal NDVI of an herb-rich forest type. As described in Chapter 3.1, the BRF data collection area was categorized as sub-xeric, indicating a dryer soil than in the compared fit [72].

The leaf reflectances in Figure 27, measured on DOY 226 and DOY 261, display the effect of the autumn which decreases the NDVIs of both dwarf shrub species. The change is more pronounce with blueberry, in which the degradation in leaf biology and leaf structure causes blueberry leaf NDVI to decrease 0.080 units, while lingonberry leaf NDVI decreases only 0.016 units. In senescence the red-edge in the beginning NIR region becomes darker and thus decreases the reflectance factor separation between red and NIR [73]. Results of previous study on the spectral effect of senescence on tree leaf reflectance [66] support the presented level of temporal change occurring in lingonberry and blueberry leaves.

NDVI705 shown in Figure 27 display a similar temporal variation as NDVI, but with a clearer separation of the species in the late summer measurements. The clearer species separation is due to the larger relative spectral contrasts of BRFs measured on 740 nm and 704 nm compared to those measured on 835 nm and 665 nm. The decrease in the contrast is induced by senescence, evident in the blueberry NDVI705 as the index decreases 0.2 units between samples measured on DOY 237 and DOY 272.

Seasonal MSI, shown in Figure 27, can be used for evaluating vegetation stress conditions related to water content, with further applications in agriculture, in drought prediction and in locating fire hazard areas. Higher MSI indicates smaller relative water content. Seasonal spectral variations of blueberry induce notable changes in MSI similar to those shown earlier with NDVI and NDVI705. In the spring samples (DOY 144, DOY 152) the contribution of the visible soil which underlies the blueberry shrubs produces MSI larger than 0.84, indicating a dry target surface. The large drop in the index at DOY 153 indicates a significant increase in the relative water content. This is related to the phenological stage of leaf growing, inducing an increase in vegetation coverage over the soil. During the summer months, blueberry MSI is around 0.50, while lingonberry produces a lower MSI of 0.37. Since earlier it was shown that the soil responses are similar between lingonberry and blueberry (Figure 22), the thicker leaves of lingonberry are considered the source of lower MSI as the lingonberry leaves hold potentially more water. The speculation of the difference in leaf water content is further supported by the leaf reflectance measurement, showing an interspecies index difference of 0.2 at DOY 226, and 0.34 at DOY 261. The highest value for blueberry leaves (MSI 0.96) indicates a water content close to zero [68].

The fourth index analysed for temporal changes was PSRI, shown in Figure 27. PSRI is an index developed especially for detecting plant senescence, but which has been noticed to be sensitive also for berry ripening. As with the three other analysed indices, blueberry shrubs show a strong change also in PSRI when moving temporally from spring to summer. The senescence is detected in the last sample with an increase of the index by 0.1 units. Lingonberry produces a relatively steady PSRI up to DOY 247, after which there is a substantial increase in index of 0.15 units. This large increase is taken as an indicator of presence of lingonberries in the sample. PSRI is normalized to wavelength of 704 nm, from which the obtained BRF is known to increase during plant senescence due to degradation of chlorophyll and the related decrease of absorption. PSRI utilizes also the difference of red (665 nm) and blue (497 nm) wavelengths, both which are known to have temporal sensitivity because of chlorophyll content. In senescence the red absorption decreases more than blue absorption, resulting an increase in the spectral

contrast and thus an increase in PSRI. The detection of lingonberries is based on the same spectral contrasts as in leaves senescence with strongly elevated BRF in red compared to blue. The shown temporal PSRI profiles in Figure 27 agree with the given literature reference [72] and traces most closely to the reference profile of a herb-rich understory type.

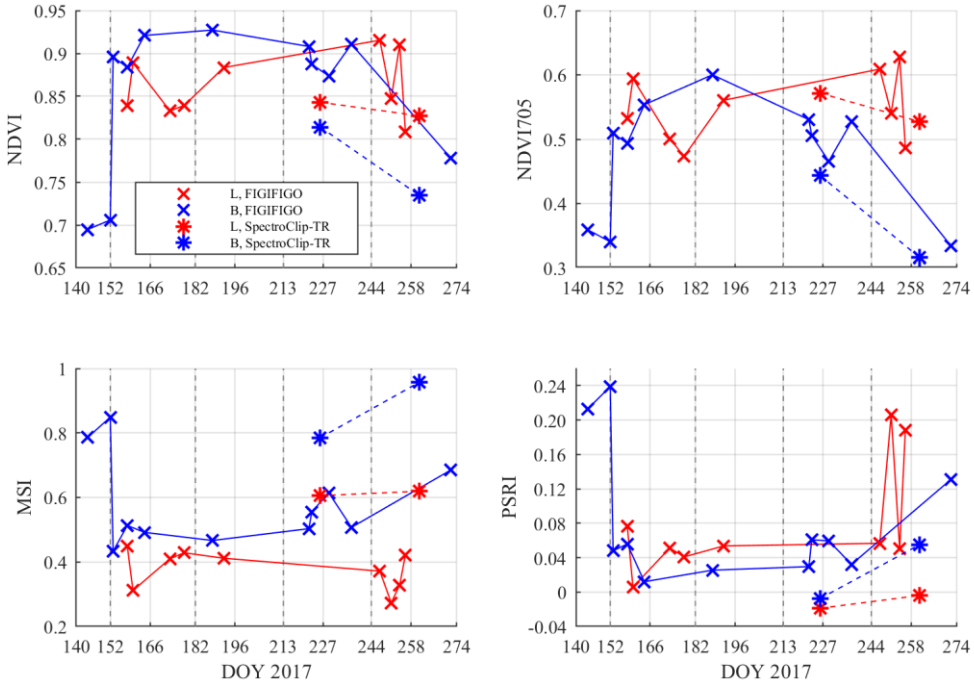

Figure 27. Four vegetation indices of blueberry and lingonberry shrubs, viewed from nadir as a function of time (Day Of Year). Illumination zenith angle is +40°.

The leaf reflectance and transmittance spectra, obtained from SpectroClip-TR measurements, are shown in Figure 28. The associated ratios (Figure 28.c , Figure 28.d) show the temporal change in the reflectances and transmittances measured from both sides of the leaves. In the shown temporal ratios, blueberry adaxial reflectance drops 80% in green, increases to 150% in red, drops to 88% at the end of the red-edge (740 nm), and increases in longer wavelengths due to decrease in water content. The VIS and NIR range spectral changes include the effects of decrease in chlorophyll content and the physical degradation of the leaf internal structure. The decrease of water content is especially prominent around the well-known water absorption peaks of 1450 nm and 1940 nm. The changes follow similar profiles for both sides but are noted stronger for adaxial side. The transmittance data shows as well seasonal variation, most profoundly in VIS region where both species exhibit a general decrease in transmittance. An exception to this can be seen in blueberry transmittance spectra, where the degradation of chlorophyll content in the leaves induces a large transmittance peak around the red wavelength (665 nm). Blueberry shows also increasing transmittance in senescence due to decrease of moisture in the leaves.

The spectra of lingonberry and blueberry in Figure 28.a and Figure 28.b agree with previously measured spectra of broadleaved trees [66], with some distinct spectral characteristic differences. The differences with lingonberry and the tree leaves include for example lingonberry leaves being brighter in reflectance in NIR by 0.06 units. Lingonberry leaves are also darker in the water absorption peak around 1450 nm by 0.02

units, indicating higher relative water content of lingonberry leaves. Blueberry leaves on the other hand are somewhat darker in reflectance in NIR, but match in the water absorption peaks. The thin blueberry leaves transmit more light through both the adaxial and abaxial sides. The difference in the blueberry leaf transmittance is especially noticeable in VIS in green wavelengths where the difference to tree leaf average is 0.08 units.

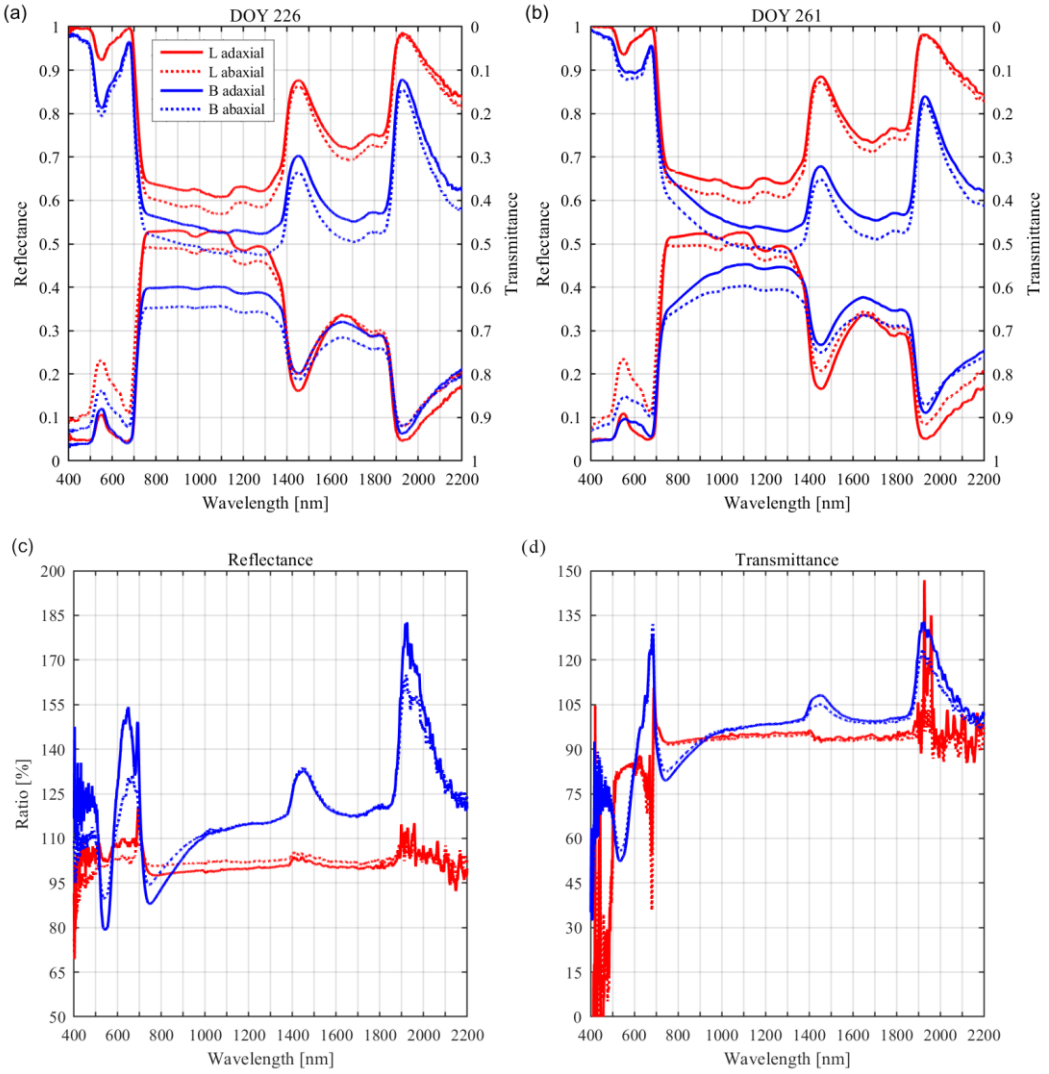

Figure 28. Averaged leaf reflectance and transmittance spectra of lingonberry and blueberry. Data collected on (a) DOY 226 (14th August) and (b) DOY 261 (18th September) of 2017. Calculated temporal ratios (DOY 261/DOY 226) of (c) reflectance and (d) transmittance.

4.4 Berry detection and component spectra

The potential of detecting dwarf shrub flowers and berries from spectral data was evaluated from calculated ratios of shrubs with products (berries or flowers) to shrubs without products (Figure 29.a). The most notable spectral changes in the shown ratios of all three samples occurred around 679 nm. The observed peaks of 320% for lingonberries, and 200% for lingonberry flowers were considered clear indicators of presence of these products. It should be noted that the abundancy of lingonberries on sample L7 (700 berries / m^2) and the relatively small number of blueberries in sample B7 (37 berries / m^2) limits the usefulness of interspecies berry detection comparison. The width of the *berry peak* is set to 100 nm with larger fraction of the difference exhibiting the left side of the peak towards red wavelengths. Another considerable spectral contrast is in blue wavelengths, between 430 nm and 495 nm, where the lingonberry flowers are shown to produce a ratio of 170%.

Following the detection of the berry peak, a spectral analysis is presented on the contributions of the shrub components to the obtained reflectance factor (Figure 29.b). The analysis includes spectral data collected of berries, leaves and soil of both species, and flowers of lingonberry. Flowers of blueberry were not measured due to low yield in the study area. Lingonberries, blueberries, and lingonberry flowers produce characteristic reflectance spectra. Lingonberries have a spectrally advanced red-edge with a steep slope starting its rise after 530 nm and continuing as steep up to 730 nm, peaking in 820 nm with BRF of 0.66. Around 970 nm water absorption band, the BRF of lingonberries drops 0.24 unit indicating a high relative water content. Blueberries have a red-edge starting spectrally at the same location as the leaves at 680 nm. The BRF peak with blueberries is 0.42 units, obtained in 910 nm. This is 90 nm further along the spectrum and 0.24 units lower compared to lingonberries. The following water absorption region around 970 nm induces a drop in BRF, similar in strength noticed previously with lingonberries.

At the berry peak in 679 nm, the averaged lingonberry leaf reflectance decreases to 0.048 units due to strong spectral absorption of the chlorophyll leaf pigment (Figure 29.b). At the same spectral location, lingonberries have reflectance of 0.39. The strength of the obtained berry peak is thus speculated to be a function of berry density.

Further spectral characteristics of the components can be identified in Figure 29.b. The berries of both species show strongly decreased reflectance factors in the water absorption regions around 970 nm, 1190 nm, 1450 nm, and 1940 nm. The berries can be considered dark compared to the leaves in longer wavelengths than 1400 nm. This gives a strong indicator that the high relative water content of berries is detectable from the spectra. The lingonberry flower spectra follow that of lingonberries in NIR and into longer wavelength up to 1750 nm, but differs strongly from berry spectrum in VIS range. Because of the strong chlorophyll absorption in the plant leaves in blue and red wavelengths, the white flowers with a red tint stand out in the ratio if the spatial coverage of the flowers is sufficiently large.

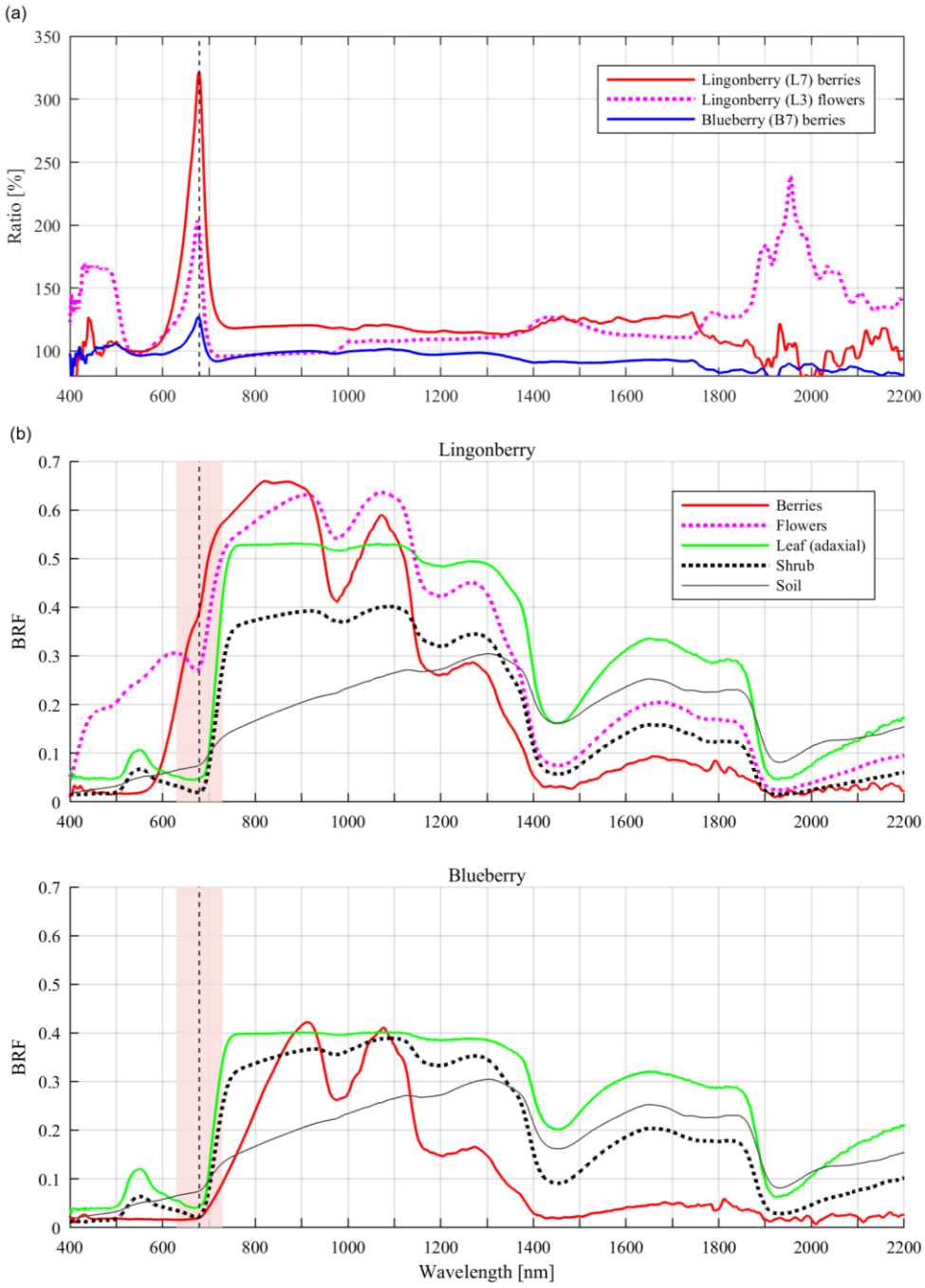

Figure 29. Lingonberry and blueberry nadir view BRFs (a) as spectral ratios of samples with flowers or berries to samples without, and (b) as averaged element wise spectra. In (b) the coloured area marks a 100 nm wide band around 679 nm. Product amounts in (a): L7 (700 berries / m^2), L3 (375 flowers / m^2), B7 (37 berries / m^2).

5 Conclusions

This thesis presented the methods and results of a research effort for spectral characterization of two highly regarded dwarf shrub species in Finland. The spectral data on lingonberry and blueberry shrubs were obtained in multidirectional measurement geometry. The included instruments were Finnish Geodetic Institute Goniospectrometer (FIGIFIGO) and SpectroClip-TR, operated in laboratory environment under artificial illumination. The spectral effects induced by the changing view and illumination angles were analysed and their impacts on the resulting reflectance factors evaluated. Multitemporal analysis, extending a period of four months, was applied by utilizing four commonly used vegetation indices to detect seasonal variation induced by the plant phenology. Further analysis was applied in evaluating the potential of berry and flower detection from the collected spectral bidirectional reflectance factor data.

In the presented anisotropy analysis, it was shown that lingonberry and blueberry shrubs have high spectral view angle dependencies over the analysed spectral range from 400 to 2200nm. Both shrub species were observed to scatter strongly into backward direction while also having noticeable specular characteristics. In the interspecies comparison, lingonberry was brighter into all view direction in the visible and near infrared wavelengths but displayed darker in the short-wave infrared. After further measurements, these characteristics were considered to arise solely from the optical properties of the leaves and shrub structures, with minimal effect from differences in the underlying soils. Heterogenous canopy structure and relatively thinner leaves of blueberry were noticed to induce higher deviation in visible wavelengths due to varying shadows. In the analysis for illumination zenith angle dependence, blueberry showed a strong response to the change while with lingonberry the response was inseparable from the associated level of uncertainty. The presented results indicate that the prospects of spectral separation between lingonberry and blueberry are improved in larger solar zeniths. The evaluated vegetation indices (NDVI, NDVI705, MSI, PSRI) all showed low spectral sensitivity to changes in the view and illumination angles in the given angular range. The same indices were further applied in temporal analysis where the shrub and leaf phenological stages from May to September were identified in all for indices, PSRI showing highest temporal contrast in berry ripening. In a further a comparative analysis of shrub samples with flowers and berries, strong contributions of the products were observed around 679 nm, and in blue wavelengths between 425 and 485 nm.

The presented results show potential for applying spectral reflectance anisotropy for identification and classification of dwarf shrub species. It was shown that the spectral discrimination of lingonberries and lingonberry flowers is possible from hyperspectral multidirectional field data obtained from a small field-of-view. Further research is suggested to be done on data acquired using unmanned aerial vehicles (UAVs) to include the constrains of angular visibility and larger spatial resolution. Other future research is suggested in form of further analysis of the obtained data on the temporal changes in soils, and in development of quantitative berry detection analysis methods. The obtained shrub and leaf spectral data are made available for others to apply in e.g. ecological studies for derivation of biophysical properties through validation of scattering models of forests, collective studies between research institutes for linking climate factors to the occurrence of dwarf shrubs and the changes in their phenology, and industry for developing improved applications to increase the exploitation of berries and to serve recreational activities.

Bibliography

[1] Mikkonen, S.; Laine, M.; Mäkelä, H. M.; Gregow, H.; Tuomenvirta, H.; Lahtinen, M.; Laaksonen, A. Trends in the average temperature in Finland, 1847 – 2013, *Stochastic Environmental Research and Risk Assessment*, 2015, vol. 29, issue 6, 1521-1529. https://doi.org/10.1007/s00477-014-0992-2

[2] Ruosteenoja, K.; Jylhä, K.; Kämäräinen, M. Climate projections for Finland under the RCP forcing scenarios, *Geophysica*, 2016, vol. 51, issue 1, 17-50. http://www.geophysica.fi

[3] Turtiainen, M.; Salo, K.; Saastamoinen O. National and regional estimates of blueberry (*Vaccinium myrtillus L.*) and lingonberry (*V. vitis-idaea L.*) yields on peatlands in Finland, *Research notes*, *SUO (Mires and peat)*, 2007, vol. 58 (3-4), 87-98

[4] Suomen luontoyrittäjyysverkosto ry, Luonnonmarjat - puolukka ja mustikka kaupallisesti tärkeimmät, *website*, www.aitoluonto.net (accessed on 13 Dec 2017)

[5] Roininen, K.; Mokkila, M. Selvitys marjojen ja marjasivuvirtojen hyödyntämispotentiaalista Suomessa, VTT report, 2007, Sitra. ISBN: 978-951-563-624-9

[6] Finnish Biodiversity Info Facility, *website*, www.laji.fi, "*Vaccinium vitis-idaea*", "*Vaccinium myrtillus*" (accessed on 13 Dec 2017)

[7] Puupponen-Pimiä, R.; Nohynek, L.; Alakomi, H.-L.; Oksman-Caldentey, K.-M. Bioactive berry compounds – novel tools against human pathogens, *Appl. Microbiol. Biotechnol.*, 2005, vol 67:8. https://doi.org/10.1007/s00253-004-1817-x

[8] Jensen J. R. *Remote Sensing of the Environment: an Earth Resource Perspective*, 2nd ed., Pearson Education, 2007, Ch. 1, 54; Ch. 11, 356; Ch. 11, 357-360; Ch. 11, 366; Ch. 12, 412; Ch. 14, 507-518; Ch. 15, 569-578. ISBN: 9780131889507

[9] Nicodemus, F. E.; Richmond, J. C.; Hsia, J. J.; Geometrical considerations and nomenclature for reflectance, National bureau of standards, US Department of commerce, 1977.

[10] Schaepman-Strub, G.; Schaepman, M. E.; Painter, T. H.; Dangel, S.; Martonchik, J. V. Reflectance quantities in optical remote sensing – definitions and case studies, *Remote Sensing of Environment*, 2006, vol. 103, 27-42. https://doi.org/10.1016/j.rse.2006.03.002

[11] Labsphere (manual), Spectralon® Diffuse Reflectance Standards, 2017. https://www.labsphere.com/

[12] Nevas, S.; Manoocheri, F.; Ikonen, E. Gonioreflectometer for measuring spectral diffuse reflectance, *Applied Optics*, 2004, vol. 43, No. 35, 6391-6399. https://doi.org/10.1364/AO.43.006391

[13] Suomalainen, J.; Hakala, T.; Peltoniemi, J.; Puttonen, E. Polarised Multiangular Reflectance Measurements Using the Finnish Geodetic Institute Field Goniospectrometer, Sensors, 2009, vol. 9, 3891-3907. ISSN: 1424-8220 https://doi.org/10.3390/s90503891

[14] Goetz, A. F. H. Making Accurate Field Spectral Reflectance Measurements, *Analytical Spectral Devices* (ASD), a review, https://panalytical.asdi.com/accurate-field-reflectance-measurements (accessed on 16 Dec 2017)

[15] Bodechtel, J.; Toselli, F.; *Imaging Spectroscopy: Fundamentals and Prospective Applications*, Springer Netherlands, 1992, p. 36. ISBN 978-0-7923-1535-3

[16] Rautiainen, M.; Lukeš, P.; Spectral contribution of understory to forest reflectance in a boreal site: an analysis of EO-1 Hyperion data, *Remote Sensing of Environment*, 2015, vol. 171, 98-104. https://doi.org/10.1016/j.rse.2015.10.009

[17] Peltoniemi, J. I.; Kaasalainen, S.; Näränen, J.; Rautiainen, M.; Stenberg, P.; Smolander, H.; Smolander, S.; Voipio, P.; BRDF measurement of understory vegetation in pine forests: dwarf shrubs, lichen, and moss, *Remote Sensing of Environment*, 2005, vol. 94, 343-354. https://doi.org/10.1016/j.rse.2004.10.009

[18] Kuusk. A.; The Hot Spot Effect in Plant Canopy Reflectance, *Photon-Vegetation Interaction*, Springer, (1991), Chapter 5 pp. 139-159, ISBN: 978-3-642-75389-3

[19] Hapke, B.; DiMucci, D.; Nelson, R.; Smythe, W.; The cause of the hotspot in vegetation canopies and soils: shadow-hiding versus coherent backscatter, *Remote Sensing of Environment*, 1996, vol.58, Issue 1, 63-68. ISSN 0034-4257 https://doi.org/10.1016/0034-4257(95)00257-X

[20] Jones, H. G.; Vaughan, R. A.; *Remote sensing of vegetation*, Oxford University Press, 2010, p. 198

[21] Sandmeier, S. R.; Itten, K. I. A Field Goniometer System (FIGOS) for acquisition of hyperspectral BRDF data, *IEEE Transactions on Geoscience and Remote Sensing*, 1999, vol. 37, No. 2, 978-986. https://doi.org/10.1109/36.752216

[22] Koechler, C.; Hosgood, B.; Andreoli, G.; Schmuck, G.; Verdebout, J.; Pegoraro, A.; Hill, J.; Mehl, W.; Roberts, D.; Smith, M. The European Optical Geometric Facility: technical description and first experiments on spectral unmixing. *IEEE, IGARSS '94*, 1994, vol. 4, 2375-2377 https://doi.org/10.1109/IGARSS.1994.399742

[23] Sandmeier, S. R. Acquisition of Bidirectional Reflectance Factor Data with Field Goniometers, *Remote Sensing of Environment*, 2000, vol. 73, 257-269. https://doi.org/10.1016/S0034-4257(00)00102-4

[24] Bruegge, C. J.; Helmlinger, M. C.; Conel, J. E.; Gaitley, B. G.; Abdou, W. A. PARABOLA III: a sphere-scanning radiometer for field determination of surface anisotropic reflectance functions, *Remote Sensing Reviews*, 2000, vol. 19, Issue 1-4. https://doi.org/10.1080/02757250009532411

[25] Painter, T. H.; Paden, B.; Dozier, J. Automated spectro-goniometer: A spherical robot for the field measurement of the directional reflectance of snow, Review of Scientific Instruments, 2003, vol. 74, No. 12. https://doi.org/10.1063/1.1626011

[26] Coburn, C. A.; Peddle, D. R. A low-cost field and laboratory goniometer system for estimating hyperspectral bidirectional reflectance, *Canadian Journal of Remote Sensing*, 2006, vol. 32, Issue 3, 244-253. https://doi.org/10.5589/m06-021

[27] Roosjen, P. P. J.; Clevers, J. G. P. W.; Bartholomeus, H. M.; Schaepman, M. E.; Schaepman-Strub, G., Jalink, H.; van der Schoor, R.; de Jong, A. A laboratory goniometer system for measuring reflectance and emittance anisotropy, Sensors, 2012, vol. 12:17358-71. https://doi.org/10.3390/s121217358

[28] Harms, J. D.; Bachmann, C. M.; Ambeau, B. L.; Faulring, J. W.; Ruiz Torres, A. J.; Badura, G.; Myers, E. Fully automated laboratory and field-portable goniometer used for performing accurate and precise multiangular reflectance measurements, Journal of *Applied Remote Sensing*, 2017, vol. 11(45). https://doi.org/10.1117/1.JRS.11.046014

[29] NASA, Airborne Multi-angle Imaging SpectroRadiometer (AirMISR), Jet Propulsion Laboratory website: https://misr.jpl.nasa.gov/Mission/airMISR/ (accessed on 14 Dec 2017)

[30] Roujean, J-L.; et al. SNORTEX (Snow Reflectance Transition Experiment): Remote sensing measurement of the dynamic properties of the boreal snow-forest in support to climate and weather forecast: Report of IOP-2008, *IGARSS 2009*, https://doi.org/10.1109/IGARSS.2009.5418231

[31] Auriol, F.; Léon, J.-F.; Balois, J.-Y.; Verwaerde, C.; François, P.; Riedi, J.; Parol, F.; Waquet, F.; Tanré, D.; Goloub, P. Multidirectional visible and shortwave infrared polarimeter for atmospheric aerosol and cloud observation: OSIRIS (Observing System Including PolaRisation in the Solar Infrared Spectrum), *Proceedings of SPIE*, 2008, Multispectral, Hyperspectral, and Ultraspectral Remote Sensing Technology, Techniques, and Applications II, 71491D. http://dx.doi.org/10.1117/12.806421

[32] Diner, D. J.; Xu, F.; Garay, M. J.; Martonchik, J. V.; Rheingans, B. E.; Geier, S.; Davis, A.; Hancock, B. R.; Jovanovic, V. M.; Bull, M. A.; Capraro, K.; Chipman, R. A.; McClain, S. C. The Airborne Multiangle SpectroPolarimetric Imager (AirMSPI): a new tool for aerosol and cloud remote sensing, *Atmospheric Measurement Techniques*, 2013, vol. 6. https://doi.org/10.5194/amt-6-2007-2013

[33] Hakala, T.; Suomalainen, J.; Peltoniemi, J. I. Acquisition of Bidirectional Reflectance Factor Dataset Using a Micro Unmanned Aerial Vehicle and a Consumer Camera, *Remote Sensing*, 2010, vol. 2, issue 3, 819-832. https://doi.org/10.3390/rs2030819

[34] Tuominen, S.; Balazs, A.; Honkavaara, E.; Pölönen, I.; Saari, H.; Hakala, T.; Viljanen, N. Hyperspectral UAV-imagery and photogrammetriccanopy height model in estimating forest stand variables, *Silva Fennica*, 2017, vol. 51, no. 5. Article id. 7721. https://doi.org/10.14214/sf.7721

[35] Roosjen, P. P. J.; Suomalainen, J. M.; Bartholomeus, H. M.; Kooistra, L.; Clevers, J. G. P. W. Mapping Reflectance Anisotropy of a Potato Canopy Using Aerial Images Acquired with an Unmanned Aerial Vehicle, *Remote Sensing*, 2017, vol. 9, Issue 5, 417. https://doi.org/10.3390/rs9050417

[36] NASA, Multi-angle Imaging SpectroRadiometer (MISR), Jet Propulsion Laboratory, *website*, https://www-misr.jpl.nasa.gov/ (accessed on 14 Dec 2017)

[37] Van Mol, B.; Ruddick, K.; The Compact High Resolution Imaging Spectrometer (CHRIS): the future of hyperspectral satellite sensors. Imagery of Oostende coastal and inland water, Presented at the *Airborne Imaging Spectroscopy Workshop, Bruges, 8 October 2004*. https://earth.esa.int/web/guest/-/the-compact-high-resolution-imaging-spectrometer-chris-the-future-of-hyperspectral-satellite-sensors-imagery-of-oostende-coastal-and-4741

[38] Lifermann, A. POLDER and Ocean Color, *website*, http://www.ioccg.org/reports/polder/polder.html

[39] Cajander, A. K. Forest types and their significance, *Acta Forestalia Fennica* (now *Silva Fennica*), 1949, vol. 56(5): 1-71. http://hdl.handle.net/10138/17982

[40] Hovi, A.; Liang, J.; Korhonen, L.; Kobayashi, H.; Rautiainen, M. Quantifying the missing link between forest albedo and productivity in the boreal zone, *Biogeosciences*, 2016, vol. 13, 6015-6030. https://doi.org/10.5194/bg-13-6015-2016

[41] Foreca, *website*, https://www.foreca.fi/Finland/Kirkkonummi, "*Past observations*". (accessed on 10 Nov 2017)

[42] Finnish Meteorological Institute, *website*, http://ilmatieteenlaitos.fi/kasvukausi-2017 (accessed on 16 Jan 2018)

[43] Suomalainen, J. Multiangular Spectroscopy and Optical Properties of Debris Covered Surfaces, *Master's thesis*, University of Helsinki, Department of Physical Sciences, 2006.

[44] Hakala, T. Improvements, Calibration, and Accuracy of the Finnish Geodetic Institute Field Goniospectrometer, *Master's thesis*, Helsinki University of Technology, Department of electronics, 2009.

[45] Peltoniemi, J. I.; Gritsevich, M.; Hakala, T.; Dagsson-Waldhauserová, P.; Arnalds, Ó.; Anttila, K.; Hannula H.-R.; Kivekäs, N.; Lihavainen, H.; Meinander, O.; Svensson, J.; Virkkula, A.; de Leeuw, G. Soot on Snow experiment: bidirectional reflectance factor measurements of contaminated snow, *The Cryosphere*, 2015, vol. 9, 1-5. https://doi.org/10.5194/tc-9-2323-2015

[46] Puttonen, E.; Suomalainen, J.; Hakala, T.; Peltoniemi, J.; Measurement of reflectance properties of asphalt surface and their usability as reference targets for aerial photos, *IEEE Transactions on Geoscience and Remote Sensing*, 2009, vol. 47, issue 7, 2330-2339. https://doi.org/10.1109/TGRS.2008.2010132

[47] SunEarthTools.com (Tools for consumers and designers of solar), *website*, https://sunearthtools.com, "*Sun position*", Used settings in the sun position calculator: coordinates 60.155736, 24.53146, year 2017, month 3, 4, 5, …, 10, day 15 (accessed on 21 Dec 2017)

[48] Savitzky, A.; Golay, M. J. E. Smoothing and Differentiation of Data by Simplified Least Squares Procedures, *Analytical Chemistry*, 1964, vol. 36, issue 8, 1627-1639. https://doi.org/10.1021/ac60214a047

[49] Suomalainen, J.; Peltoniemi, J.; Hakala, T. Measurement and Analysis of Bidirectional Reflectance, seminar presentation, *Seminar at Avances en espectro-radiometría*, 2009, "Conferencia_7_Juha_Suomalainen.pdf", http://www.congresos.cchs.csic.es/seminarioradiometria/content/documentos (accessed on 22 Dec 2017)

[50] Hovi, A.; Forsström, P.; Mõttus, M.; Rautiainen, M. Evaluation of accuracy and practical applicability of methods for measuring leaf reflectance and transmittance spectra, *Remote Sensing*, 2018, vol. 10, issue 1, 25. https://doi.org/10.3390/rs10010025

[51] Hovi, A.; Raitio, P.; Rautiainen, M.; A spectral analysis of 25 boreal tree species, *Silva Fennica*, 2017, vol. 51, No. 4, p. 16. https://doi.org/10.14214/sf.7753

[52] Mõttus, M.; Hovi, A.; Rautiainen, M. Theoretical algorithm and application of a double-integrating sphere system for measuring leaf transmittance and reflectance spectra, *Applied Optics*, 2017, vol. 56, No. 3. https://doi.org/10.1364/AO.56.000563

[53] Stenberg, P.; Mõttus, M.; Rautiainen, M. Photon recollision probability in modelling the radiation regime of canopies — A review, *Remote Sensing of Environment*, 2016, vol. 183, 98-108. http://dx.doi.org/10.1016/j.rse.2016.05.013

[54] Hatchell, D. C. (editor) Analytical Spectral Devices, *Technical Guide, 3rd edition*, 1999.

[55] Sandmeier, S.; Müller, C.; Hosgood, B.; Andreoli, G. Physical Mechanism in Hyperspectral BRDF Data of Grass and Watercress, *Remote Sensing of Environment*, 1998, vol. 66, 222-233. https://doi.org/10.1016/S0034-4257(98)00060-1

[56] Jackson, R. D.; Teillet, P. M.; Slater, P. N.; Fedosejevs, G.; Jasinski, M. F.; Aase, J. K.; Moran, M. S. Bidirectional Measurements of Surface Reflectance for View Angle Corrections of Oblique Imagery*, Remote Sensing of Environment*, 1990, vol. 32, 189-202. https://doi.org/10.1016/0034-4257(90)90017-G

[57] Rouse, J. W.; Haas, R. H.; Schell, J. A.; Deering, D. W. Monitoring vegetation systems in the great plains with ERTS, 1974, *Goddard Space Flight Center 3d ERTS-1 Symp., vol. 1, sect. A, 309-317*

[58] Gitelson, A.; Merzlyak, M. N. Spectral Reflectance Changes Associated with Autumn Senescence of Aesculus hippocastanum L. and Acer platanoides L. Leaves. Spectral Features and Relation to Chlorophyll Estimation, *Journal of Physiology*, 1994, vol. 143(3), 286 – 292. https://doi.org/10.1016/S0176-1617(11)81633-0

[59] Rock, B. N.; Williams, D. L.; Vogelmann, J. E.; Hoshizaki, T. Field and airborne spectral characterization of suspected acid deposition damage in red spruce (*Picea rubens*) from Vermont. *Proceedings of the 11th International Symposium on Machine Processing of Remotely Sensed Data*, 1985, Purdue University

[60] Rock, B. N.; Williams, D. L.; Vogelmann, J. E.; Hoshizaki, T. Remote Detection of Forest Damage, *BioScience*, 1986, vol. 36, No. 7 439-445. https://doi.org/10.2307/1310339

[61] Merzlyak, M. N.; Gitelson, A. A.; Chivkunova, O. B.; Rakitin, V. Yu. Non-destructive optical detection of pigment changes during leaf senescence and fruit ripening, *Physiologia Plantarum*, 1999, vol. 106, 135-141

[62] Sims, D. A.; Gamon, J. A. Relationships between leaf pigment content and spectral reflectance across a wide range of species, leaf structures and developmental stages, *Remote Sensing of Environment*, 2001, vol. 81, 337-354.

[63] Gates, D. M.; Keegan, H. J.; Schleter, J. C.; Weidner, V. R. Spectral properties of plants, *Applied Optics*, 1965, vol. 5, issue 1, 11-20. https://doi.org/10.1364/AO.4.000011

[64] Sandmeier, S. 2004 Variability of BRDF / Spectral BRDF. In von Schönermark, M.; et al. (Eds.), *Reflection Properties of Vegetation and Soil* (1st ed.). 136, 139-146. ISBN: 3-89685-565-4. Wissenschaft und Technik Verlag. 2004

[65] Lukeš, P.; Stenberg, P.; Rautiainen, M.; Mõttus, M.; Vanhatalo, K. M. Optical properties of leaves and needles for boreal tree species in Europe, *Remote Sensing Letters*, 2013, 4:7, 667-676. https://doi.org/10.1080/2150704X.2013.782112

[66] Raitio, P. Comparison of tree species spectra and their utilization in remote sensing, *Master's thesis*, Aalto University, School of Engineering, Department of Built Environment, 2017

[67] Ross, J.; Marshak, A. The influence of leaf orientation and the specular component of leaf reflectance on the canopy bidirectional reflectance, *Remote Sensing of Environment*, 1989, vol. 27, issue 3, 251-260. https://doi.org/10.1016/0034-4257(89)90086-2

[68] Hunt, R. E., Jr; Rock, B. N. Detection of changes in leaf water content using near- and middle-infrared reflectances, *Remote Sensing of Environment*, 1989, vol. 30, issue1, 43-54. https://doi.org/10.1016/0034-4257(89)90046-1

[69] Schlerf, M.; Hill, J.; Koetz, B.; Kneubuehler, M. Retrieving canopy structure from hyperspectral multi-angular satellite data, *5th EARSeL SIG IS workshop Imaging Spectroscopy: Innovation in Environmental Research, Bruges, Belgium,* 2007. https://earth.esa.int/web/guest/document-library

[70] Vanderbilt, V. C.; Grant, L. Plant Canopy Specular Reflectance Model, *IEEE Transactions on Geoscience and Remote Sensing,* 1985, vol. GE-23, No. 5, 772-730. https://doi.org/10.1109/TGRS.1985.289390

[71] Wang, J.; Chen, Y.; Chen, F.; Shi, T.; Wu, G. Wavelet-based coupling of leaf and canopy reflectance spectra to improve the estimation accuracy of foliar nitrogen concentration, *Agricultural and Forest Meteorology*, 2018, vol. 248, 306-315. https://doi.org/10.1016/j.agrformet.2017.10.017

[72] Rautiainen, M.; Mõttus, M.; Heiskanen, J.; Akujärvi, A.; Majasalmi, T.; Stenberg, P. Seasonal reflectance dynamics of common understory types in a northern European boreal forest. *Remote Sensing of Environment*, 2011, vol. 115, issue 12, 3020-3028. https://doi.org/10.1016/j.rse.2011.06.005

[73] Demarez, V.; Gastellu-Etchegorry, J. P.; Mougin, E.; Marty, G.; Proisy, C.; Dufréne, E.; Le Dantec, V. Seasonal variation of leaf chlorophyll content of a temperate forest. Inversion of the PROSPECT model, *International Journal of Remote Sensing*, 1999, vol. 20, issue 5, 879-894. https://doi.org/10.1080/014311699212975

Appendix A: Photographs of measured samples

Measured samples were photographed from nadir view for documentation purposes. The shown photos act as recordings of the sample structures and of the applied illumination.

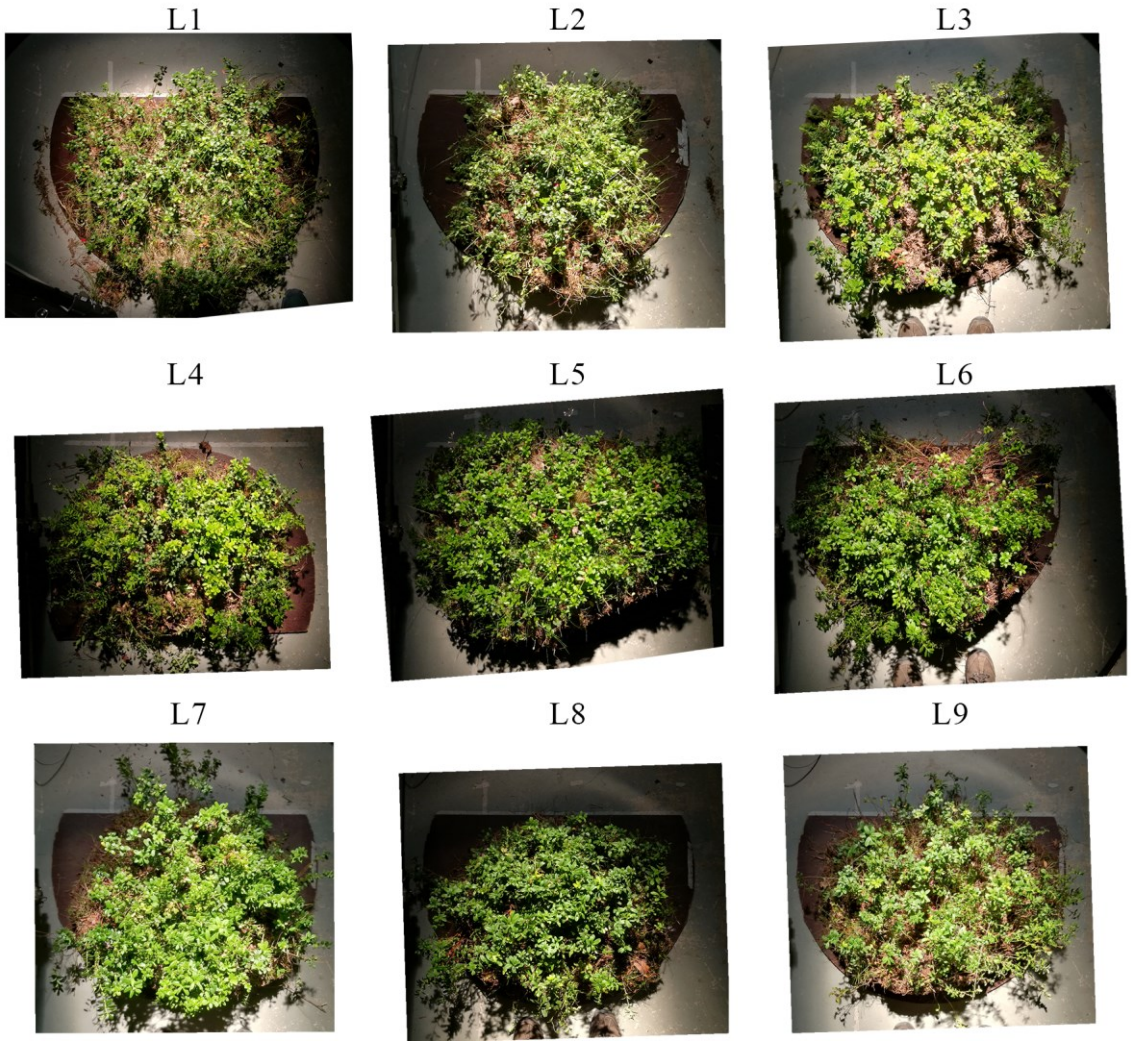

Figure A1. Nadir view photographs of nine lingonberry samples. Photos taken with a smartphone camera using automatic camera settings.

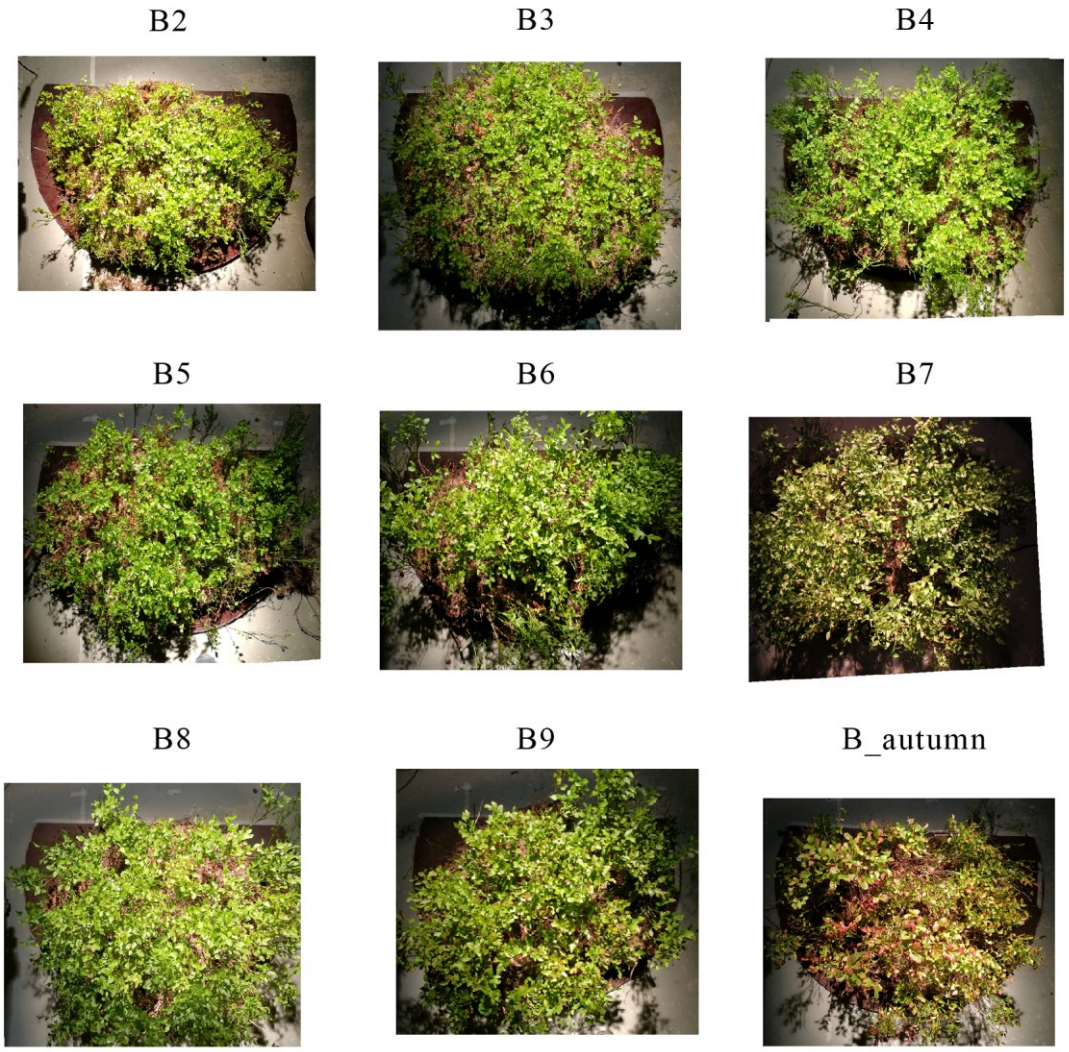

Figure A2. Nadir view photographs of nine blueberry samples. Photos taken with a smartphone camera using automatic camera settings.

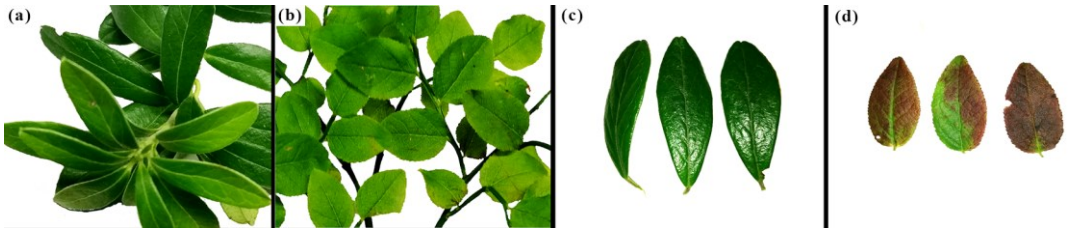

Figure A3. Photographs showing a selection of (a, b) lingonberry leaves and (b, d) blueberry leaves that were measured for reflectance and transmittance. Photos (a) and (b) represent the leaves measured on 14 August while (c) and (d) represent the autumn leaves measured on 18 September.